Published in final edited form as:
Geol Soc Am Bull. 2020 ; 132(1-2): 17–30. doi:10.1130/b35185.1.

Deposition of >3.7 Ga clay-rich strata of the Mawrth Vallis Group, Mars, in lacustrine, alluvial, and aeolian environments

Donald R. Lowe[1,†], **Janice L. Bishop**[2], **Damien Loizeau**[3,4], **James J. Wray**[5], **Ross A. Beyer**[2]

[1]Department of Geological Sciences, Stanford University, Stanford, California 94305-2115, USA

[2]SETI & NASA-Ames Research Center, Mountain View, California, USA

[3]Université Claude Bernard Lyon 1, Ens de Lyon, CNRS, UMR 5276 LGL-TPE, F-69622, Villeurbanne, France

[4]Institut d'Astrophysique Spatiale, Université Paris Sud, F-91405 Orsay, France

[5]School of Earth and Atmospheric Sciences, Georgia Institute of Technology, Atlanta, Georgia 30332-0340, USA

Abstract

The presence of abundant phyllosilicate minerals in Noachian (>3.7 Ga) rocks on Mars has been taken as evidence that liquid water was stable at or near the surface early in martian history. This study investigates some of these clay-rich strata exposed in crater rim and inverted terrain settings in the Mawrth Vallis region of Mars. In Muara crater the 200-m-thick, clay-rich Mawrth Vallis Group (MVG) is subdivided into five informal units numbered 1 (base) to 5 (top). Unit 1 consists of interbedded sedimentary and volcanic or volcaniclastic units showing weak Fe/Mg-smectite alteration deposited in a range of subaerial depositional settings. Above a major unconformity eroded on Unit 1, the dark-toned sediments of Unit 2 and lower Unit 3 are inferred to represent mainly wind-blown sand. These are widely interlayered with and draped by thin layers of light-toned sediment representing fine suspended-load aeolian silt and clay. These sediments show extensive Fe/Mg-smectite alteration, probably reflecting subaerial weathering. Upper Unit 3 and units 4 and 5 are composed of well-layered, fine-grained sediment dominated by Al-phyllosilicates, kaolinite, and hydrated silica. Deposition occurred in a large lake or arm of a martian sea. In the inverted terrain 100 km to the NE, Unit 4 shows very young slope failures suggesting that the clay-rich sediments today retain a significant component of water ice. The MVG provides evidence for the presence of large, persistent standing bodies of water on early Mars as well as a complex association of flanking shoreline, alluvial, and aeolian systems. Some of the clays, especially the Fe/Mg smectites in upper units 1 and 2 appear to have formed through subaerial weathering whereas the aluminosilicates, kaolinite, and hydrated silica of units 3, 4, and 5 formed mainly through alteration of fine sediment in subaqueous environments.

[†] drlowe@stanford.edu.

INTRODUCTION

The Mawrth Vallis region of Mars is known both for the prominent outflow valley from which it gets its name (Fig. 1) and for the wide presence of phyllosilicate-rich rocks formed during the Noachian Period, 4.1–3.7 Ga (Michalski and Noe Dobrea, 2007; Loizeau et al. 2012). The abundance of phyllosilicate minerals in Noachian rocks across the surface of Mars was revealed by OMEGA (Observatoire pour la Minéralogie, l'Eau, les Glaces et l'Activité) on board Mars Express (Poulet et al., 2005; Bibring et al., 2006) and by the Compact Reconnaissance Imaging Spectrometer for Mars (CRISM) on board the Mars Reconnaissance Orbiter (e.g., Murchie et al., 2009; McKeown et al., 2009; Bishop et al., 2008a, 2011, 2013a; Bishop and Rampe, 2016). These studies have shown that phyllosilicate-bearing rocks include two contrasting assemblages of phyllosilicate minerals: a basal sequence over 100 m thick of Fe/Mg smectite-bearing rocks and an overlying unit variously estimated at 50–60 m thick containing Al-bearing phyllosilicates and hydrated silica (Bishop et al., 2008a; Loizeau et al., 2010; Noe Dobrea et al., 2010, 2011). Because the formation of phyllosilicate minerals requires the presence of water (e.g., Chamley, 1989), their abundance in Noachian rocks has been taken by some to indicate the existence of a more clement early climate, including the presence of liquid water at the surface (e.g., Poulet et al., 2005; Mustard et al., 2008; Bristow and Milliken, 2011; Carter et. al., 2015; Bishop et al., 2018). The origin(s) of these phyllosilicate-bearing rocks have been widely discussed in terms of the climate and surface conditions of early Mars and/or hydrologic and diagenetic conditions in the martian subsurface (e.g., Poulet et al., 2005; Loizeau et al., 2007, 2010; Wray et al., 2008, 2009, 2010; Bishop et al., 2008a; Mustard et al., 2008; McKeown et al., 2009; Michalski et al., 2010; Noe Dobrea et al., 2011; Gou et al., 2015).

In the Mawrth Vallis region (Fig. 1), the phyllosilicate-rich rocks, here informally termed the Mawrth Vallis Group (MVG), are well displayed on the walls of a small crater, Muara, just west of Mawrth Vallis (Figs. 2 and 3). The oldest part of the MVG (Fig. 4) is characterized by Fe/Mg smectite alteration (Figs. 5A, 5B). It is overlain across a transition zone by 50–70 m of rocks rich in Al-phyllosilicates and hydrated silica and a complex variety of other minerals (Bishop et al., 2013a, 2016). The Al-phyllosilicate-rich unit is overlain in most areas by a thin, younger caprock of largely unaltered pyroxene-bearing mafic volcanic rocks (Loizeau et al., 2007).

The implications of these rocks toward the nature of the early martian climate is complicated by the uncertain origins of the rocks themselves and of the included phyllosilicates. These layered clay-rich rocks have been variously interpreted as weathering products of crustal rocks or sediments under surface conditions (Noe Dobrea et al., 2010; Farrand et al., 2014; Bishop and Rampe, 2016), as detrital phyllosilicate sediments deposited in a large martian sedimentary basin (Wray et al., 2008), or alteration products formed through widespread hydrothermal and/or diagenetic processes (Ehlmann et al., 2011; Noe Dobrea et al., 2010; Sun and Milliken, 2015). They have also been attributed to precipitation from magmatic fluids moving upwards during the last-stage degassing of the martian interior (Meunier et al., 2012).

The present study examines the MVG in two areas in the Mawrth Vallis region (Fig. 1): (1) around the walls of Muara crater (Figs. 2 and 3) just west of Mawrth Vallis and (2) in an area of so-called inverted terrain ~100 km north-east of Muara crater and east of Mawrth Vallis. The objective of this study is to better characterize the internal stratigraphy of the phyllosilicate-rich layers, to evaluate the processes and conditions under which they formed, and to assess whether they represent a wetter early Mars or some other combination of conditions less removed from those prevailing today.

METHODOLOGY

The geologic interpretations developed here utilize grayscale images of the martian surface provided by the High Resolution Imaging Science Experiment (HiRISE) camera (McEwen et al., 2010). The images have been enlarged and examined using a range of brightness, contrast, and sharpening options, but otherwise, unless specified, individual figures are unenhanced. Both study areas have stereo images available and the anaglyph images have been used as well as available digital terrain maps. All references to the relative tone of outcrops (e.g., light-toned, dark-toned, etc.) are to the grayscale tones as seen in the HiRISE images and the specific figures included in this paper. The distance and length scales used are those provided on the HiRISE images. Single pixels on the HiRISE images are 25–50 cm across; CRISM spectral images have a resolution of 18 m/pixel or more.

Determining the strike and dip of layering in the walls of Muara crater has been problematic. Bedding attitudes along the north and northwest walls, where the present study is focused, have been discussed by Wilhelm et al. (2013). Their conclusion was that the structural complexity in this area makes it difficult to evaluate dip magnitudes and directions but their figure 2 shows dips averaging ~20–25 degrees, mostly toward the crater center. However, this is also roughly the magnitude and direction of the topographic slope in this area and the more linear, slope-perpendicular outcrop pattern of units is not consistent with rocks dipping parallel or nearly parallel to the topographic slope. Most small, simple craters show nearly flat to outward dips of crater-wall strata (Melosh, 1989). We have attempted to estimate dips from bed deflection where the beds cross topography and from HiRISE images adjusted to show views along the crater walls. These results suggest roughly flat-lying strata. Our estimates of unit thickness are based on the strata being horizontal.

The spectral approaches and methodologies are summarized by Murchie et al. (2009), Loizeau et al. (2010), and Bishop et al. (2013a). The present study has involved spectral analysis of CRISM image FRT000094F6 (Figs. 5 and 6), which has been calibrated with the Map-projected Targeted Reduced Data Records (MTRDR) technique (Seelos, 2011). Spectral parameters (Viviano-Beck et al., 2014) were used to identify regions of specific compositions and spectra (0.4–4 μm) were acquired from several sites in each region to confirm phyllosilicate identifications as in previous studies (e.g., Bishop et al., 2008a, 2013a; Bishop and Rampe, 2016).

The accuracy of orbital interpretations of martian geology can be problematic but have been tested where rovers have explored the same portion of the surface (Stack et al., 2016; Williams et al., 2018). The main shortcoming in these comparisons is that rovers are

confined to low-relief terrain whereas the best stratigraphic and sedimentological details are generally provided by higher-relief areas where cliffs show internal stratigraphic details and erosional topography can reflect internal architecture. In general, many larger-scale sedimentologically useful details can be seen in high-quality orbital images but finer, more detailed analyses at scales below 1 or 2 m require ground-based images (Stack et al., 2016).

SPECTRAL ANALYSIS

Spectral images of Muara crater and their interpretation in terms of the main phyllosilicate minerals present are shown in Figures 5 and 6. Examples of CRISM spectra of the dominant three compositional units are shown in Figure 6. Mapped in green (Fig. 5B) are spectra consistent with short-range ordered aluminosilicates such as allophane and imogolite containing an OH overtone band near 1.39–1.40 μm, a broad H_2O combination band centered near 1.92 μm, and a broad OH combination band near 2.19–2.20 μm (Bishop et al., 2013b; Bishop and Rampe, 2016). This unit is observed at the top of the phyllosilicate-bearing units as shown in Figure 5C. Mapped in blue (Fig. 5B) are spectra consistent with Al-phyllosilicates such as montmorillonite and halloysite/kaolinite or opal. These spectra are characterized by an OH overtone band at 1.41 μm, a H_2O combination band at 1.91 μm that is narrower than in the upper unit, and an OH combination band centered near 2.20–2.21 μm (Fig. 6). This blue unit is present above the red unit and below the green unit (Fig. 5C). Finally, mapped in red is a larger portion of the phyllosilicate-bearing outcrop (Fig. 5C) that is characteristic of Mg-bearing nontronite or Fe-bearing saponite because the spectral features fall between those of nontronite and saponite (Bishop et al., 2008a). Example spectra from this red unit (Fig. 6) exhibit features similar to nontronite and ferrosaponite including an OH overtone band at 1.42 μm, a H_2O combination band at 1.91 μm, an OH combination band centered near 2.29 μm, and an additional OH band near 2.39 μm.

MUARA CRATER

Muara is a small, roughly circular impact crater ~3.8 km in diameter centered at ~24.3°N and 340.7°W (19.3°E) (Figs. 1 and 2). It is covered by HiRISE images ESP_012873_2045 and PSP_004052_2045, which form a stereo pair. The crater is a simple, bowl-shaped crater with a rim that reaches ~300 m above the crater floor. The HiRISE images show surface features strongly suggesting the presence of layered sedimentary and/or volcanic rocks around the crater walls (Figs. 3) and spectral features are present in CRISM image FRT000094F6 indicating the presence of phyllosilicates (Fig. 5).

The floor of Muara is covered by a field of wind-generated sand dunes ~2.5 km across (Figs. 2 and 3). Spectral images show no phyllosilicates in the dunes. Similar low albedo, pyroxene-bearing deposits throughout the region have been interpreted as aeolian or pyroclastic deposits composed of volcanic sand (Loizeau et al., 2007). The dune crests are elongate generally ENE-WSW. Dune geometry suggests wind from the SSE toward the NNW. The dune field has an irregular edge and is surrounded on the north side of the crater by a fringe of post-cratering sedimentary deposits interspersed with outcrops of the MVG (Fig. 7). The sedimentary deposits in this fringe include patches of dark windblown sand, chaotic landslide deposits, and water-worked deposits that include what appear to be well-

developed, contour-parallel gravel beach ridges (Fig. 7). A variety of small channels is present including some eroded into MVG bedrock and others cutting across the older landslides (Fig. 7). These features attest to an early history of wall collapse, water runoff, and accumulation of debris in a lake on the crater floor following crater formation.

Illumination at the time HiRISE images were collected was from the SSW and the best exposed and structurally least complicated section of the MVG along the northwestern and northern crater wall is taken as the type section (Fig. 8). Based on tone, texture, and structuring, the 200–250 m of exposed section are here divided into five stratigraphic units, numbered units 1 through 5 from base upward (Figs. 4 and 8). The dark caprock that overlies the MVG contains pyroxene (Loizeau et al., 2007), lacks phyllosilicates, and probably represents unaltered volcanic and/or volcaniclastic rocks.

Unit 1

Description—Unit 1, making up the lower half of the walls of Muara crater, is a succession of medium-toned rocks at least 100 m thick with the base not exposed. These rocks are well stratified in most exposures and in the CRISM image show a weak Fe/Mg-smectite alteration except for the uppermost 30–50 m, which show an intense Fe/Mg smectite alteration (Fig. 5C). Stratification in Unit 1 ranges from thin layers 1–2 m or less in thickness (Fig. 9A) to crude layering at a scale of 5–10 m thick (Figs. 9B, 9C). Overall, the lower half of Unit 1 is more finely layered than the upper half. On the lower part of the northern and NW crater wall, fine layering is locally well developed (Fig. 9A). These relatively thin, even, tabular layers are continuous for at least 100 m along strike with no evidence of internal scour or erosion. In other areas, there appears to be abundant large-scale cross-stratification (Fig. 9A). There is common large-scale thickening, thinning, and wedging of units and there are a number of internal erosion surfaces (Figs. 9A, 9C, and 10A). The upper third to half of Unit 1 around most of Muara Crater crops out as massive to thickly bedded, intensively fractured rock (McKeown et al., 2013) broken into blocks from <1 m to ~20 m across (Figs. 8 and 10B). Crude layering is often visible through the fracturing (Fig. 10B) and it is possible that the rock itself is more finely layered.

Interpretation—The upper 30–50 m of Unit 1 appear to represent the lower part of the Fe/Mg smectite zone of previous investigators (e.g., Bishop et al., 2013a). However, the bulk of Unit 1 shows only weak Fe/Mg smectite alteration (Fig. 5). Based on the presence of plagioclase and pyroxene in this and other dark units in Muara crater and vicinity (Poulet et al., 2008; Viviano and Moersch, 2013), the widely developed stratification, and the alteration of the rock to Fe/Mg smectite, we would infer that the more crudely layered parts of Unit 1, such as much of the section on the east crater wall, may represent altered mafic or ultramafic volcanic flows and/or volcaniclastic units. Previous studies of alteration and clay formation in this area have also assumed that these rocks represent a basaltic sequence (e.g., Zolotov and Mironenko, 2016). The fine, even layering in the lower part of Unit 1 (Fig. 9A) suggests that some parts may have been deposited in standing bodies of water and the association of these layers with large-scale cross-stratification (Fig. 10A) and channel-like features (Fig. 9A) may indicate that overall the lower part of Unit 1 represents a complex of interfingering alluvial, fluvial, aeolian, and/or lacustrine environments. The more crudely stratified upper

half of Unit 1 that shows undulating layering and some large-scale cross-stratification on the northern and NW wall of the crater may represent largely windblown sediments.

Unit 2

Description—Above Unit 1 across an irregular and probably unconformable contact is up to 35 m of medium- to dark-toned, well stratified rock of Unit 2 (Figs. 3, 8, and 11). The base forms a distinct break around the crater wall between underlying, massive, fractured rock of Unit 1 and overlying, dark-toned, stratified rock of Unit 2 (Fig. 8). Unit 2 varies in thickness from 0, where Unit 3 rests directly on Unit 1, to ~35 m. These variations in thickness probably reflect in large part the highly irregular surface on which Unit 2 was deposited. This contact may be the regional unconformity identified by Loizeau et al. (2012) as a “paleo-surface” within the MVG sequence. The best exposures of Unit 2 in Muara crater occur along the NW crater wall, although there is some young dark windblown sediment masking portions of the rock in this area and layering in the lower part of Unit 2 may be better developed than can be seen in the HiRISE images (Fig. 11).

Along the NW wall, the outcrop of Unit 2 shows a series of parallel, sharp-crested ridges, 20–50 m wide and a few meters high, that run up-and-down the crater wall, roughly perpendicular to contours and the strike of bedding (Fig. 11). The bottoms of the round-bottomed swales between ridges are widely coated by dark windblown sand (Fig. 11). The ridges are elongated parallel to the wind direction up the crater wall, show bedrock layering throughout, and were apparently cut into bedrock by the prevailing wind.

Overall, Unit 2 consists of well-stratified rock made up of lenticular, interfingering light-, medium-, and dark-toned layers from <0.5 to perhaps 2 or 3 m thick. Locally, the lowest few meters of Unit 2 are very dark-toned, massive to weakly stratified rock (Fig. 11). Upward, well-developed stratification is defined by complexly interfingering lighter streaks and lenses up to ~1 m thick, a few discontinuous blocky layers, medium-toned layers up to ~2 m thick, and thin, very dark layers mostly <1 m thick. The thin dark layers are mostly overlain or underlain by thin light-toned beds (Fig. 11). Most layers persist for less than 100 m along the outcrop (Fig. 11).

Interpretation—Unit 2 shows an intense Fe/Mg-smectite spectral signature (Fig. 5C). Modeling estimates of the unit containing spectral features near 2.3 μm indicate 30–70 vol% Fe/Mg-smectite (Poulet et al., 2014). We infer that Unit 2 represents a sedimentary sequence, although some blocky-weathering units may be thin mafic lava flows. Interbedded layers probably include dark, reworked volcaniclastic debris derived in large part by erosion of the underlying rocks of Unit 1 and possibly pyroclastic materials. The thin, lenticular dark layers overlain by light layers are more prominent in Unit 3 and will be discussed there, but are thought to represent windblown sand layers (darkest) capped by thin very fine-grained layers of windblown dust (light). A few peaked, lenticular, very dark layers may represent dunes of windblown sand (Fig. 11). All bed-scale units are highly lenticular and at least one surface within Unit 2 along the northern wall appears to cut down through a few meters of underlying material, but overall there is no evidence for large-scale scour, erosion, or steeply inclined layering. The abundance of lenticular, dark-, and light-toned layers and couplets is

consistent with an aeolian origin, especially toward the top where the dark-light alternation is most prominent. There may also be a component of water-worked sediments in the medium-toned units, but there is no clear evidence for aqueous transport, such as erosional channels, and all layers could be composed of windblown components.

Unit 3

Description—Unit 3 is a transitional unit, 20–30 m thick, of well-stratified, mainly medium- to light-toned rock between the top of the predominantly dark-toned, layered rocks of Unit 2 and the very light-toned rocks of Unit 4 (Figs. 8, 11, and 12). Much of Unit 3 shows well-developed layering down to the resolution of the HiRISE images, indicating that it is stratified at scales to or below ~50 cm. The base of Unit 3 is locally an erosional unconformity (Fig. 11) along which as much as 5 m of strata of the underlying Unit 2 are truncated. The lower half of Unit 3 in the NW crater wall consists of prominently banded units showing either post-depositional deformation or syndepositional stratigraphic complexity (Fig. 11). Dark-toned layers in this zone, where thicker, are commonly lenticular or show pinch-and-swell (Fig. 11). They also widely exist as thin, very continuous layers probably mostly <50 cm thick that coat both unconformities and the boundaries of virtually all light-toned units. Dark-toned layers lack evidence for internal layering, although their low albedo may simply make internal stratification difficult to see. Interbedded light-toned layers are generally thicker, more continuous, and often underlie or drape the dark layers (Fig. 11). The light layers commonly show even finer internal layering down to the resolution of the HiRISE images.

The boundary between the Fe/Mg smectite zone and the overlying Al-phyllosilicate layer appears to fall within Unit 3 (Fig. 5D), although the lower resolution of the CRISM images and uncertainties in correlating HiRISE and CRISM images would also allow the boundary to coincide roughly with the Unit 2–3 contact.

Interpretation—We would suggest that the dark layers in the lower half of Unit 3 represent windblown sand that was commonly swept into dunes but is widely distributed and/or preserved as thin, more tabular layers. If the dark layers represent sand-sized windblown bed-load sediment, the draping light-toned caps are probably silt to clay-sized debris deposited during the waning stages of dust storms as well as during periods of reduced wind activity between storm events. An especially good example of this close association of lenticular, dark-toned dune sands and light fine-sediment drapes can be seen on the north crater wall in the lower part of Unit 3 (Fig. 12). Mixed medium-toned layers may represent either stacks of very thin alternating light- and dark-toned layers or of mixtures of hydraulically equivalent dark sand grains and light clay aggregates.

It is not clear whether the undulating layers and truncated units in the lower part of Unit 3 represent deformation in response to an external event, such as an impact, or whether it is entirely of depositional origin involving erosion, draping of irregular surfaces, deposition of lenticular layers, and perhaps minor sliding. However, we suspect that all of these features are sedimentary in origin because no clearly deformational features are present, such as

over-steepened beds (dips greater than the angle of repose), overturned or recumbent layers, isolated blocks (slides), or truncation of overlying layers by underlying ones.

Above this lower zone of dunes, drapes, and complex bedding, the upper part of Unit 3 is a zone of evenly stratified light- or medium-toned rock (Fig. 12). There is a rather cyclic interlayering of light layers ~1–3 m thick and thin, <50-cm-thick dark- or medium-toned layers. The light layers locally show a very fine, even, flat internal layering at the resolution of the HiRISE images. The thinness and evenness of the layering, the predominance of phyllosilicate minerals and the implied fine grain size, and absence of scour features suggest deposition under low energy, possibly subaqueous conditions. In some areas, flat, even bedding passes laterally into curved, upward-peaked layering that resembles inferred dunes lower in Unit 3 (Fig. 12).

Unit 4

Description—Unit 4 is the prominent 20–25-m-thick light-toned band around the upper part of the crater wall. This part of the crater wall is a zone of extensive fracturing, including both closely spaced sets of more-or-less orthogonal fractures that sweep across the crater wall (Fig. 13), probably related to the impact that formed Muara crater, and large, cross-cutting fractures and faults. There also appears to be a change in northern-crater-wall slope roughly coincident with the Unit 3–4 contact and there may be fractures at this point formed during downslope sliding and slumping. Fractures at all scales are marked by accumulations of medium- to dark-toned material and the smaller fracture sets subdivide the rock into small rectangular blocks a few meters across that are separated by thin septa of dark material. We infer that the fractures are marked by more easily erodible materials and/or were open and have been widely filled by dark windblown sand. There is also a host of irregular lines and features across the crater wall at all scales that could be fractures, joints, small faults, layering, or other features within the rock, but for which, in many cases, a specific origin remains elusive.

The intersection of bedding and fracture sets has widely resulted in the downslope slippage of fracture-bounded blocks, forming a jagged, saw-tooth geometry (Figs. 12 and 13). Windblown dark sand has filled the fractures and more horizontal surfaces formed by block sliding (Fig. 13).

Interpretation—Overall, Unit 4 is characterized by bedded, light-toned rock interrupted by very thin laminations of darker material. This unit correlates with the Al-phyllosilicate-rich layer observed in CRISM images (Fig. 5C). As with the upper part of Unit 3, it appears to have been deposited mainly as fine-grained sediment.

Bedding can be difficult to distinguish in Unit 4 because of the uniformly light-toned character and paucity of layers of contrasting tone or color. The spaced dark laminations seen on the crater wall may be sedimentary layers but others may be accumulations of modern windblown sand along crevices and on ledges following bedding. These suggest layering on the scale of 1–3 m thick. Layers appear to be tabular with no clear undulations, dune-shaped features, or scours/channels. Finer-scale layering has been widely observed in other areas (Loizeau et al., 2010) and, if the light-toned layers in Unit 4 are similar to those

in Unit 3, then the thick light layers are also most likely made up of much thinner layers. We would also infer deposition of the fine silts and clays of Unit 4 in a subaqueous environment.

Unit 5

Description—Unit 5, the uppermost member of the MVG in the crater-wall sequence, is laterally heterogeneous and the outcrop widely disrupted by impact processes and crater-wall collapse. On the northwestern wall (Fig. 8), there is a reasonably well-exposed section. It includes a basal zone of dark rock that widely produces debris that covers and obscures the Unit 4–5 contact. Above this zone, Unit 5 consists of interfingering and interlayered dark and medium- to light-toned layers for a total Unit 5 thickness of ~25–30 m.

Interpretation—The dark, more friable layers that yield abundant slope-mantling debris most probably represent mafic flows, mafic volcaniclastic layers, and/or windblown sediment composed of mafic sand grains. The light-toned layers are thought to be layers of phyllosilicate-rich clays and silts and poorly crystalline materials. This interlayering suggests that the sedimentation of the light-toned units was interrupted by volcanic episodes or floods of volcaniclastic sediment, although details of the internal makeup of these layers cannot be resolved. CRISM images indicate that Unit 5 contains poorly crystalline aluminosilicate phases similar to allophane and imogolite (Fig. 5D).

INVERTED TERRAIN

Surface Features

About 100 km north-northeast of Muara crater (Fig. 1) is an area of irregular terrain in which dark, sinuous features that resemble channels cross broad, lighter areas (Fig. 14). When examined closely, it is seen that the “channels” are topographically high plateaus and the intervening lighter areas are broad, open valleys. This topography has been referred to as inverted topography because one hypothesis for its origin is that it started as a flatter landscape crossed by channels that were later filled with resistant volcanic rock or sedimentary materials. Subsequent erosion left the more resistant “channel fill” standing in relief above the more easily eroded surrounding materials that form today’s valley floors (Loizeau et al., 2007; Noe Dobrea et al., 2010).

The present study lies within an area of inverted terrain at ~26°N and 18.5°W, Oxia Pallis Quadrangle, and is covered by the stereo pair of HiRISE images ESP_013361_2060 and ESP_013084_2060. It is in the northwest part of a large valley bounded by channel-like plateaus to the north and west (Figs. 14, 15, and 16). These are capped by flat-lying, medium- to dark-toned, well-cratered rock, probably basalt, and local patches of dark windblown dunes. The elevation difference between the valley bottom and flat-topped plateau is ~25–30 m. The light-toned valley floor is made up of essentially flat-lying, light material. The cliff-forming unit, which is composed of interbedded dark- and light-toned units with a dark caprock forming the plateau surface, appears to be roughly equivalent to Unit 5 of the MVG and the caprock at Muara crater and the underlying light-toned, valley-floor unit to Unit 4, although precise correlation across this distance is uncertain. The base of Unit 4 in the inverted terrain is not exposed within the HiRISE images used.

The valley floor (Fig. 16) slopes down from west to east at ~4° to 6° and appears to be underlain by light-toned Unit 4 rock, possibly interbedded with thin layers of dark-toned material: dark layers are interbedded with light-toned layers in the valley wall, but these are not apparent on the valley floor. Part of the valley floor is marked by step-like elongate zones of rubble up to ~40 m wide separated by areas of smoother light topography (Fig. 16). The smooth light-toned surfaces are covered either by very fine, featureless material, possibly bedrock or a regolith cover, or by finely patterned ground (Fig. 16). Adjacent to the dark debris aprons at the bases of the bounding cliffs, dark material has been swept into small dunes. In contrast, dunes of light-toned material are essentially absent. The polygons making up the patterned ground are mostly 1–4 m across, although smaller polygons may be present below the resolution of the images.

The rubbly zones bear a strong resemblance to many terrestrial landslides and debris flows formed by slope failure (Fig. 17). In the study area on Mars, their formation appears to have involved failure of the surface layers of the light-toned rock, collapse and brecciation, but with only minor downslope movement. Most rubbly areas show a distinct, arcuate head scarp or series of arcuate scarps on the upslope side. Down-dropped blocks immediately below the head scarp are often large and broken by additional fractures along which the downslope side has been further down-dropped. Above the head scarp in some areas are arcuate dark lines parallel to the head scarp that appear to represent fractures that have not yet evolved into failures (Fig. 16). Within the rubble zones, brecciation tends to become more chaotic from the head scarp to the downslope tip: the blocks tend to become smaller, more jumbled, and do not fit together. The distal 5–10 m of the slides widely consist of blocks only 1–3 m across embedded in a matrix of fine material, probably representing debris flows (Fig. 16). Shadowing of the sharp downslope ends of the chaotic zones indicates a terminal drop-off. There are many areas that do not display these exact size trends and some slides have coarser material toward the tips but these general trends are widespread.

These features suggest that the rubble areas formed by decoupling of the light-toned rock layers, possibly along dark layers, and some downslope sliding of the detached layers, with normal faulting and fragmentation of the upslope parts of the detached mass of material and increasing amounts of flow and brecciation toward the fronts of the slides. The frontal zones of the slides often mixed and became debris flows. These features are well developed in many modern terrestrial landslides (Fig. 17). In some areas, the slides appear to have collapsed, thinned, and lost much of their volume (Fig. 16, point f). Such areas include abundant dark sediment.

In several areas, localized failure has formed irregular, disconnected patches of rubble without major downslope movement of the fractured debris. In the small rubbly patch shown in Figure 18, a detached mass of light-toned material has fragmented internally, in part along the boundaries of polygons in the surficial patterned ground, and slid only a short distance downslope, forming a distinct rubble front along the downslope side. There is an upslope scarp and larger proximal blocks but no clear downslope zone of mixed, debris-flow material. The central part of this rubble has further collapsed in two areas (Fig. 18), each marked by a distinct, dark-toned topographic low area that extends to the edge of the failure.

One shows a small debris-flow tongue extending beyond the rubble zone onto the edge of the adjacent light, patterned ground (Fig. 18). The dark areas are interpreted to expose or be partially covered by dark sediment, possibly from dark layers, and the light collapsed layer is greatly thinned or missing in these low areas. Many of the rubbly areas have narrow, dark, topographically low zones along their fronts and extending downslope (Fig. 18). These locally show the accumulation of dark sediment along their courses, small dark debris cones right up against the rubble fronts, and isolated light-toned blocks. Some of these topographically low areas appear to represent small runoff channels.

Origin of the Patterned Ground

While impact-generated joints are widespread in the areas studied, such as along the upper walls of Muara (Fig. 13), the small polygons that widely cover areas of flatter ground underlain by Unit 4 in both study areas are most likely either thermal contraction fractures (Mellon, 1997; Mellon et al., 2008), like those formed widely in terrestrial glacial and peri-glacial settings, or desiccation contraction fractures. Based on criteria discussed by Levy et al. (2009), evidence for the wholesale collapse of the light layers, and features suggesting that collapse was locally accompanied by flowing water, we would infer that the patterned ground in the study area formed mainly by thermal contraction associated with a layer of permafrost. Others have interpreted these structures as desiccation cracks (El-Maarry et al., 2014) but unlike most desiccation cracks, those in the study area are very uniform in size and shape, most 0.5–4 m across, and include only one size of visible crack and bounding joints, not a hierarchy of crack types common to desiccation fractures (El-Maarry et al., 2014). The presence of expandable smectite clays in Unit 4 upon which polygons are widely developed may suggest that desiccation as well as thermal contraction, ice wedging, and sublimation influenced their formation.

Controls on Failure and Mass Movement

The wide distribution of patterned ground, the collapse and thinning of the light-toned layers within the slides, and the apparent evolution of water during sliding suggest that the light layers contain abundant water ice and probably permafrost at a shallow depth. The polygons formed before the mass movement as shown by the fact that in many places the polygon boundaries served as the loci of fracturing and breakage of the light layers into blocks during collapse and sliding (Figs. 16 and 18). Because exposed ice cannot survive at the martian surface, the surface of the light-toned “bedrock” and permafrost layers is probably mantled by non-icy debris. A similar debris and vegetative layer characterizes most terrestrial permafrost terrains. Because these light-toned areas and the light regolith at the surface are widely characterized by aluminous clays, we would suggest that the light-toned layers consist mainly of a mixture of phyllosilicates and water ice. At the surface, the water has been lost through sublimation until a solid, protective layer of light clay, phyllosilicates, and other rocky debris has formed.

We infer that the rubble zones formed as a result of partial melting of the permafrost at a shallow depth (Fig. 19). As the ice melted, the overlying sedimentary and regolith layers were destabilized, decoupled from the underlying layers, fractured, and locally slid. Water appears to have run out through more porous layers, perhaps the dark layers, and/or via the

fractures, carrying some of the fine dark sand and silt. Fracturing associated with collapse exposed additional permafrost to sublimation and/or melting, promoting continued fracturing, downslope movement, and head scarp retreat.

Within many of the rubbly areas, the fractured light-toned layers have thinned and largely disappeared during collapse, probably through increased sublimation of water ice within the more intensely fractured rock. The latitude of the inverted terrain study area (26°N) is close to the lower latitude of 30°N for permafrost and polygon development (Head et al., 2003) and ground ice may be periodically subject to freeze-thaw cycles during martian summers. This would be consistent with the inferred runoff features seen associated with Unit 4 areas of fracturing and collapse and perhaps even more likely under different, recent climatic conditions at higher obliquity (e.g., Forget et al., 2006). Our results suggest that the light-toned layers are mixtures of phyllosilicates, silt, and water ice. This interpretation is consistent with the observation that the light layers yield little or no coarse debris to form windblown dunes or talus slopes: they tend to break into large blocks during fracturing and then break down rapidly through sublimation and melting of the included water into very fine-grained silt and clay.

Age of Surface Features in the Inverted Terrain

The rubble zones and patterned ground in the inverted terrain study area show evidence of a very young origin. There are very few craters across the valley surface. The patterned ground is sharp and fresh in most areas and probably formed relatively recently perhaps over the last few million years during periods of climatic instability (Head et al., 2003). The patterned ground polygons are cut and disturbed by the processes of failure, sliding, and mass movement to form the rubbly zones, further indicating an even more recent origin of the mass transport events.

DISCUSSION

Composition of the Mawrth Vallis Group

We interpret the Mawrth Vallis Group as a stratigraphic sequence within which the layers are primarily of sedimentary origin. The bulk of units 2 through 5 can be described in terms of two main end-member sediment types represented by the dark- and light-toned materials.

(1) The dark-toned sediment is well represented in Muara crater where dark sand makes up the modern dune field on the crater floor and sand patches on the crater walls, and where dark beds in the Noachian MVG show common pinch-and-swell and dune-like features and geometries in cross section. Deposits at the bases of cliffs are composed almost exclusively of fine, dark-toned material, locally swept up into small dark dunes. The similarity of all of these dark-toned sedimentary layers, including their apparent fine granularity and presence of dune-like bedforms, suggests that most are composed of sand- to fine gravel-sized material, probably representing reworked and eroded volcanic material. Most appear to represent windblown sand.

Wind-generated sand dunes are among the most widespread sedimentological features on Mars (Grotzinger et al., 2005), both at the surface and in the geologic record, so their

development in Muara crater and the MVG is not unexpected. There are many studies of martian aeolian deposits, most focused on dunes that provide 3-D outcrops, including smaller, rover-based exposures, than the MVG studied here (e.g., Grotzinger et al., 2005; Milliken et al., 2014; Banham et al., 2018).

(2) Upper Unit 3 in Muara crater and Unit 4 in both study areas are composed primarily of light-toned materials. Because these light-toned layers correspond to the distribution of aluminosilicate clays, they are probably composed largely of clay and silt- to fine sand-sized phyllosilicate particles. The common draping of dark-toned dune-like bedforms by thin light-toned layers and fine interlayering of the two sediment types in units 2 and 3 are consistent with the interpretation that the dark layers represent windblown sand and the light layers are composed of sediment deposited out of suspension, often forming drapes, during periods of reduced wind or current activity. Higher in Unit 3 and in parts of Unit 4, light-toned sediment shows widespread fine layering and tabular geometries consistent with deposition of very fine silt and clay under quiet, subaqueous conditions. However, ripped up silt- and sand-sized chunks of light-toned sediment may have formed sparse dunes that are largely indistinguishable in the uniformly light sediment as seen in upper Unit 3 (Fig. 12). Medium-toned layers may be mixtures of both light- and dark-toned particles. Studies in the inverted terrain suggest that today the light-toned layers are mixtures of fine sediment and water ice, a conclusion consistent with HiRISE observations of near surface ice in mid-latitude regions (Dundas et al., 2018).

Depositional Evolution of the MVG

If the dark-toned layers in units 2 and 3 are composed mostly of windblown sand, their environment of deposition was mainly subaerial. The upward increase in the proportion of light-toned layers through units 2, 3, and 4 in Muara crater offers two possibilities: (1) upper Unit 3 and Unit 4 are parts of a gradually expanding regional subaerial loess plain, perhaps along the margins of a drying ocean or large lake that occupied the lowlands along the eastern edge of Chryse Planitia, or (2) there is a transition from subaerially deposited windblown sediment in Unit 2 and the lower part of Unit 3 to subaqueously deposited sediment in the upper part of Unit 3 and Unit 4. Both scenarios are consistent with the light layers having been composed largely of fine-grained clay, silt, and very fine-grained sand. The thin, even, fine layering down to the resolution of the HiRISE images in the light-toned layers is consistent with deposition under low-energy conditions with little scour or erosion. However, loess deposits are typically massive, homogeneous, and accumulate to thicknesses of many meters with little or no internal layering (e.g., Pye, 1995). We would suggest that the features of the light-toned layers of upper Unit 3, Unit 4, and parts of Unit 5 are most consistent with sedimentation by the settling of silt and clay out of a water column in a large lake or sea. With the possible exception of the stratigraphically complex zone at the base of Unit 3, deposition took place under very quiet, subaqueous conditions. The presence of some sweeping, dune-like strata in upper Unit 3 suggests that the lake/sea floor may have been periodically exposed with fluctuations in water level and that the exposed lake margins were sites of wind activity and the construction of small dunes or deposition of fine suspended silt and clay eroded from the exposed clay-rich lake beds.

The stratigraphically complex interval at the base of Unit 3 includes erosive surfaces, truncations, onlap surfaces, and a complex interlayering of dark and light sediments. This stratigraphically complex deposit may mark a coastal zone where the largely terrestrial sequence of Unit 2 interfingers with the largely lacustrine/ocean sequence of upper Unit 3. Wave and current activity could have locally been at a maximum within this zone and it could also have been a zone of local erosion during falls in water level. This zone is also roughly coincident with the contact between the lower Fe/Mg-smectite zone and upper Al-phyllosilicate zone in CRISM images. This narrow contact zone is locally characterized by a spectral signature indicating an abundance of Fe^{+2}-bearing components (Bishop et al., 2013a) in contrast to the phyllosilicate-rich units on either side. We suggest that this zone includes shoreface sediments composed mainly of winnowed, unaltered mafic minerals worked and deposited within the coastal zone represented by lower Unit 3. The presence of jarosite along this horizon (Bishop et al., 2016) is also consistent with the development of local coastal evaporitic ponds.

Origin of the Phyllosilicates in the MVG

The presence of pyroxene and plagioclase is consistent with Unit 1 being composed largely of basalt or a similar mafic or ultramafic volcanic rock and associated volcaniclastic sediments. There is a low level of Fe/Mg-smectite alteration throughout the middle and lower parts of Unit 1. Alteration in the bulk of Unit 1 does not seem to form discrete layers. Sun and Milliken (2015) have argued that Fe/Mg smectite alteration is more widespread in rocks exposed in central peak uplifts of craters in Noachian terrain across Mars than Al-phyllosilicate rocks and that this Fe/Mg smectite alteration appears to have originated at depth within the mafic volcanic crust and was brought to the surface during uplift of the central peaks. In the absence of any visible clay stratigraphy in the middle and lower parts of Unit 1 and the widespread and deep record of Fe/Mg smectite alteration across broad areas of Noachian terrain, we would suggest that the Fe/Mg smectite alteration of rocks of the middle and lower parts of Unit 1 occurred under the influence of deep diagenetic or hydrothermal fluids. However, the absence of minerals characteristic of high-temperature alteration, such as Mg-rich clays, chlorite, serpentine, prehnite, and chlorite (e.g., Ehlmann et al., 2011) implies that the unit was not altered at elevated temperatures (Michalski et al., 2015; Bishop et al., 2018).

The upper part of Unit 1, Unit 2, and lower Unit 3 show intense Fe/Mg smectite alteration (Fig. 5C). All of these units are made up in large part of layers inferred to represent detrital, sand-sized, mafic volcaniclastic debris, but their greater degree of alteration in comparison to lower parts of Unit 1 suggest either that they were affected by different processes of alteration and/or that the processes were similar but more intense. Our results suggest that this intense alteration originated through subaerial weathering associated with the unconformity at the top of Unit 1 and, subsequently, of debris derived from erosion of Unit 1 during deposition of Unit 2.

In Unit 2 and lower Unit 3 mafic dark-toned sediments are interbedded with layers of light-toned material. Based on spectral data, light-toned layers in upper Unit 3 and Unit 4 are interpreted to be Al-phyllosilicate-rich layers. The resolution of the CRISM images is lower

than that of the HiRISE images and we cannot determine at this stage whether the thin, light-toned layers in Unit 2 and lower Unit 3 are also composed of Al-phyllosilicates interbedded with dark Fe/Mg-smectite layers, as we suspect, or whether they are light toned but also show Fe/Mg smectite alteration.

The light-toned rocks of upper Unit 3 and units 4 and 5 are dominated by aluminous clays and hydrated silica that must have formed before the fresh volcanic caprock was emplaced. Much of the layering in these units is flat, even, and tabular, consistent with the deposition of fine sediment under subaqueous conditions. The presence of layers of dark, sand-sized sediment interlayered with light, Al-phyllosilicate rocks in Unit 3 confirms that wholesale regional hydrothermal alteration did not form the phyllosilicates in situ from a single, compositionally uniform protolith since adjacent layers would have suffered similar degrees of alteration. The interstratification of contrasting sediment types further argues against the formation of the entire MVG as an extraordinarily thick soil zone during weathering at the top of Unit 4 or Unit 5. Unit 4 can be traced over wide areas in the Mawrth Vallis region and appears to have a sheet-like geometry, parallel in general to layering in other MVG rocks, suggesting that all represent depositional stratigraphic units and not hydrothermal alteration zones.

Our results suggest that the Al-phyllosilicates in units 2, 3, 4, and 5 of the MVG could have formed (1) elsewhere and were transported to their present sites of deposition as fine windblown grains, (2) through water runoff from surrounding land areas, or (3) in situ through the alteration of fine silt- to clay-sized clastic grains transported into a body of water by wind, as would be the case for volcanic dust and ash. All of these processes may have been involved in forming the final Mawrth Vallis Group sediments, as occurs in and around modern terrestrial oceans and lakes (e.g., Bristow and Milliken, 2011).

CONCLUSIONS

The Mawrth Vallis Group is here subdivided into five informal stratigraphic units numbered 1 (base) through 5 (top). Unit 1 consists of what we infer to be interlayered and interfingering volcaniclastic strata and locally volcanic flows. The sedimentary rocks show evidence of deposition under a range of conditions that included aeolian, fluvial/alluvial, and quiet, possibly subaqueous environments. The surface of Unit 1, below Unit 2, is irregular and in some places Unit 2 appears to be absent, suggesting that the top of Unit 1 is an erosional unconformity and that Unit 2 has locally accumulated as valley fill between highs of Unit 1 rock. This surface may represent a major paleosol characterized by Fe/Mg smectite alteration that extends several tens of meters into the top of Unit 1.

Unit 2 and lower Unit 3 form a transition from the dark bedrock of Unit 1 to the flat-layered, fine-grained, muddy, subaqueous depositional settings represented by sedimentary rocks of upper Unit 3 and Unit 4. Unit 2 appears to be dominated by mafic volcaniclastic debris derived from Unit 1 and perhaps some thin, late-stage volcanic flows. Upward in Unit 2, its initially massive, dark-toned character is increasingly interrupted by thin lenses of light-toned sediment, which often drape undulating surfaces. We suggest that this association of dark lenticular units draped by light-toned layers represents windblown layers composed of

mafic sand-sized sediment that are overlain and/or underlain by light-toned layers deposited as finer, suspended windblown sediment. Deposition of upper Unit 2 and lower Unit 3 occurred on the lower parts of an alluvial surface with increasing proximity to water and to potential sources of windblown silt and clay eroded from exposed basinal sediments.

In Muara crater, the thickness and proportion of light-toned layers increases upward through Unit 2 and into Unit 3. The accompanying upward thinning of the dark layers and thickening of the light layers suggests a transition from mainly aeolian sand deposition (dark) to the deposition of fine-grained dust and clays (light). This transition is locally marked by a zone of stratigraphic complexity in lower Unit 3, including channels eroded several meters into underlying strata, and widespread interlayering of dark windblown sand and thicker, finely laminated dust deposits. There is a zone of Fe^{+2}-rich deposits that may mark a zone of hydraulic concentration of more resistant, heavy mineral phases, such as occurs on terrestrial beaches and coastal zones.

Most of the light-toned layers in the upper part of Unit 3 and lower Unit 4 are tabular, with only a few, very thin dark layers. The abundance of phyllosilicates suggested by CRISM data, the continuity and evenness of layering, the wide presence of fine flat layering down to the resolution of the HiRISE images, and paucity of evidence for coarse sediments and features suggesting high levels of current activity, such as visible erosional features, all suggest deposition in a quiet subaqueous setting. This could have been a large lake or arm of a sea. The interlayering of thick dark and light layers in Unit 5 suggests the possible alternation of mafic volcanic and volcaniclastic events with continuing subaqueous deposition of clay-rich sediments.

Our results suggest that the MVG phyllosilicates formed in three main settings: (1) the weak, widely distributed Fe/Mg smectite alteration of middle and lower Unit 1 is thought to reflect low-temperature diagenetic to hydrothermal alteration. (2) The intense Fe/Mg smectite alteration in uppermost Unit 1, Unit 2, and lower Unit 3 formed by alteration at the martian surface during accumulation of the sequence, probably through subaerial weathering of mafic materials and lithic grains. (3) The Al-phyllosilicates of upper Unit 3 and Unit 4 may include some clay blown into a sea or lake by the wind and some material carried across fluvial systems from surrounding areas of weathering. However much probably formed by in situ alteration of airborne dust and volcanic ash on and below the bottom of a large lake or sea.

We note that all of the inferred phyllosilicate-rich sediments of units 2, 3, 4, and 5 of the MVG are light toned. Most pure kaolinite and smectite clays on Earth are white to very pale, whereas terrestrial shales and mudstones of all ages and representing virtually all depositional settings are dark toned. The latter, of course, reflects the presence of reduced organic matter. If these martian clay-rich deposits lack organic matter, either the lake or ocean in which they were deposited was characterized by environmental conditions that precluded the existence of life forms and/or the accumulation of dark organic matter, such as some extreme evaporitic environments, or life had not evolved on Mars at 3.7 Ga, when these sediments were deposited.

The results of this study suggest that water was widespread in Noachian surface environments on Mars, probably as precipitation, streams, standing bodies of water including lakes and/or seas, and in the subsurface. Future studies in stratigraphically complex areas like the Mawrth Vallis Group will add to our understanding of the complexity, distribution, and persistence of these water-rich environments on early Mars and whether or not they hosted early martian life.

ACKNOWLEDGEMENTS

National Aeronautics and Space Administration (NASA) Mars Data Analysis Program grant no. NNX12AJ33G provided support for this project. D. Lowe received additional support from Stanford University, Stanford, California, USA. J. Bishop and J. Wray also received support from the NASA Astrobiology Institute. D. Loizeau received support from the European Research Council under the European Union's Seventh Framework Program (FP7/2007–2013)/ERC grant agreement no. 280168 and under the H2020-COMPET-2015 program (grant 687302). The authors thank C. Gross for assistance with Figure 5 and M. Day and one anonymous reviewer for many helpful comments on the manuscript.

REFERENCES CITED

Banham SG, Gupta S, Rubin DM, Watkins JA, Sumner DY, Edgett KS, Grotzinger JP, Lewis KW, Edgar LA, Stack-Morgan KM, Barnes R, Bell JF III, Day MD, Ewing RC, Lapotre MGA, Stein NT, Rivera-Hernandez F, and Vasaveda AR, 2018, Ancient Martian aeolian processes and paleomorphology reconstructed from the Stimson formation on the lower slope of Aeolis Mons, Gale crater, Mars: Sedimentology, v. 65, p. 993–1042, 10.1111/sed.12469.

Bibring J-P, Langevin Y, Mustard JF, Poulet F, Arvidson R, Gendrin A, Gondet B, Mangold N, Pinet P, and Forget F, 2006, Global mineralogical and aqueous Mars history derived from OMEGA/Mars Express data: Science, v. 312, p. 400–404, 10.1126/science.1122659. [PubMed: 16627738]

Bishop JL, and Rampe EB, 2016, Evidence for a changing Martian climate from the mineralogy at Mawrth Vallis: Earth and Planetary Science Letters, v. 448, p. 42–48, 10.1016/j.epsl.2016.04.031.

Bishop JL, Noe Dobrea EZ, McKeown NK, Parente M, Ehlmann BL, Michalski JR, Milliken RE, Poulet F, Swayze GA, Mustard JF, Murchie SL, and Bibring J-P, 2008a, Phyllosilicate diversity and past aqueous activity revealed at Mawrth Vallis, Mars: Science, v. 321, p. 830–833, 10.1126/science.1159699. [PubMed: 18687963]

Bishop JL, Lane MD, Dyar MD, and Brown AJ, 2008b, Reflectance and emission spectroscopy study of four groups of phyllosilicates: Smectites, kaolinite-serpentines, chlorites and micas: Clay Minerals, v. 43, p. 35–54, 10.1180/claymin.2008.043.1.03.

Bishop JL, Saper L, Beyer RA, Lowe DR, Wray JJ, McKeown NK, and Parente M, 2011, Possible sedimentary features in phyllosilicate-bearing rocks at Mawrth Vallis, Mars: 42nd Lunar and Planetary Science Conference, March 7–11, The Woodlands, Texas, USA, Lunar and Planetary Institute, no. 2374, 2 p.

Bishop JL, Loizeau D, McKeown NK, Saper L, Dyar MD, Des Marais D, Parente M, and Murchie SL, 2013a, What the ancient phyllosilicates at Mawrth Vallis can tell us about possible habitability on early Mars: Planetary and Space Science, v. 86, p. 130–149, 10.1016/j.pss.2013.05.006.

Bishop JL, Rampe EB, Bish DL, Baker LL, Abidin Z, Matsue N, and Henmi T, 2013b, Spectral and hydration properties of allophane and imogolite: Clays and Clay Minerals, v. 61, p. 57–74, 10.1346/CCMN.2013.0610105.

Bishop JL, Gross C, Rampe EB, Wray JJ, Parente M, Horgan B, Loizeau D, Viviano-Beck CE, Clark RN, Seelos FP, Ehlmann BL and Murchie SL, 2016, Mineralogy of layered outcrops at Mawrth Vallis and implications for early aqueous geochemistry on Mars: 47th Lunar Planetary Science Conference, March 21–25, The Woodlands, Texas, USA, Lunar and Planetary Institute, abstract no. 1332.

Bishop JL, Fairén AG, Michalski JR, Gago-Duport L, Baker LL, Velbel MA, Gross C, and Rampe EB, 2018, Surface clay formation during short-term warmer and wetter conditions on a largely cold ancient Mars: Nature Astronomy, v. 2, p. 206–213, 10.1038/s41550-017-0377-9.

Bristow TF, and Milliken RE, 2011, Terrestrial perspective on authigenic clay mineral production in ancient Martian lakes: Clays and Clay Minerals, v. 59, p. 339–358, 10.1346/CCMN.2011.0590401.

Carter J, Loizeau D, Mangold N, Poulet F, and Bibring J-P, 2015, Widespread surface weathering on early Mars: A case for a warmer and wetter climate: Icarus, v. 248, p. 373–382, 10.1016/j.icarus.2014.11.011.

Chamley H, 1989, Clay Sedimentology: New York, USA, Springer-Verlag, 623 p., 10.1007/978-3-642-85916-8.

Dundas CM, Bramson AM, Ojha L, Wray JJ, Mellon MT, Byrne S, McEwen AS, Putzig NE, Viola D, Sutton S, Clark E, and Holt JW, 2018, Exposed subsurface ice sheets in the Martian mid-latitudes: Science, v. 359, p. 199–201, 10.1126/science.aao1619. [PubMed: 29326269]

Ehlmann BL, Mustard JF, Murchie SL, Bibring J-P, Meunier A, Fraeman AA, and Langevin Y, 2011, Subsurface water and clay mineral formation during the early history of Mars: Nature, v. 479, p. 53–60, 10.1038/nature10582. [PubMed: 22051674]

El-Maarry MR, Watters W, McKeown NK, Carter J, Noe Dobrea E, Bishop JL, Pommerol A, and Thomas N, 2014, Potential desiccation cracks on Mars: A synthesis from modeling, analogue-field studies, and global observations: Icarus, v. 241, p. 248–268, 10.1016/j.icarus.2014.06.033.

Farrand WH, Glotch TD, and Horgan B, 2014, Detection of copiapite in the northern Mawrth Vallis region of Mars: Evidence of acid sulfate alteration: Icarus, v. 241, p. 346–357, 10.1016/j.icarus.2014.07.003.

Forget F, Haberle RM, Montmessin F, Levrard B, and Head JW, 2006, Formation of glaciers on Mars by atmospheric precipitation at high obliquity: Science, v. 311, p. 368–371, 10.1126/science.1120335. [PubMed: 16424337]

Gou S, Yue Z, Di K, and Wang J, 2015, Mineral abundances and different levels of alteration around Mawrth Vallis, Mars: Geoscience Frontiers, v. 6, p. 741–758, 10.1016/j.gsf.2014.09.004.

Grotzinger JP, Arvidson RE, Bell JF III, Calvin W, Clark BC, Fike DA, Golombek M, Greeley R, Haldemann A, Herkenhoff KE, Jolliff BL, Knoll AH, Malin M, McLennan SM, Parker T, Soderblom L, Sohl-Dickstein JN, Squyres SW, Tosca NJ, and Watters WA, 2005, Stratigraphy and sedimentology of a dry to wet eolian depositional system, Burns formation, Meridiani Planum, Mars: Earth and Planetary Science Letters, v. 240, p. 11–72, 10.1016/j.epsl.2005.09.039.

Head JW, Mustard JF, Kreslavsky MA, Milliken RE, and Marchant DR, 2003, Recent ice ages on Mars: Nature, v. 426, p. 797–802, 10.1038/nature02114. [PubMed: 14685228]

Levy J, Head J, and Marchant D, 2009, Thermal contraction crack polygons on Mars: Classification, distribution, and climate implications from HiRISE observations: Journal of Geophysical Research. Planets, v. 114, E01007, 10.1029/2008JE003273.

Loizeau D, Mangold N, Poulet F, Bibring J-P, Gendrin A, Ansan V, Gomez C, Gondet B, Langevin Y, Masson P, and Neukum G, 2007, Phyllosilicates in the Mawrth Vallis region of Mars: Journal of Geophysical Research. Planets, v. 112, E08S08, 10.1029/2006JE002877.

Loizeau D, Mangold N, Poulet F, Ansan V, Hauber E, Bibring JP, Gondet B, Langevin Y, Masson P, and Neukum G, 2010, Stratigraphy in the Mawrth Vallis region through OMEGA, HRSC color imagery and DTM: Icarus, v. 205, p. 396–418, 10.1016/j.icarus.2009.04.018.

Loizeau D, Werner SC, Mangold N, Bibring J-P, and Vago JL, 2012, Chronology of deposition and alteration in the Mawrth Vallis region, Mars: Planetary and Space Science, v. 72, p. 31–43, 10.1016/j.pss.2012.06.023.

McEwen AS, Banks ME, and Baugh N, et al., 2010, The High Resolution Imaging Science Experiment (HiRISE) during MRO's Primary Science Phase (PSP): Icarus, v. 205, p. 2–37, 10.1016/j.icarus.2009.04.023.

McKeown NK, Bishop JL, Noe Dobrea EZ, Ehlmann BL, Parente M, Mustard JF, Murchie SL, Swayze GA, Bibring J-P, and Silver E, 2009, Characterization of phyllosilicates observed in the central Mawrth Vallis region, Mars, their potential formational processes, and implications for past climate: Journal of Geophysical Research. Planets, v. 114, 10.1029/2008JE003301.

McKeown NK, Bishop JL, and Silver EA, 2013, Variability of rock texture and morphology correlated with the clay-bearing units at Mawrth Vallis, Mars: Journal of Geophysical Research. Planets, v. 118, p. 1245–1256, 10.1002/jgre.20096.

Mellon MT, 1997, Small-scale polygonal features on Mars: Seasonal thermal contraction cracks in permafrost: Journal of Geophysical Research. Planets, v. 102, p. 25617–25628, 10.1029/97JE02582.

Mellon MT, Arvidson RE, Marlow JJ, Phillips RJ, and Asphaug E, 2008, Periglacial landforms at the Phoenix landing site and the northern plains of Mars: Journal of Geophysical Research. Planets, v. 113, E00A23, 10.1029/2007JE003039.

Melosh HJ, 1989, Impact Cratering: A Geologic Process: New York, USA, Oxford University Press, 245 p.

Meunier A, Petit S, Ehlmann BL, Dudoignon P, Westall F, Mas A, El Albani A, and Ferrage E, 2012, Magmatic precipitation as a possible origin of Noachian clays on Mars: Nature Geoscience, v. 5, p. 739–743, 10.1038/ngeo1572.

Michalski JR, and Noe Dobrea EZ, 2007, Evidence for a sedimentary origin of clay minerals in the Mawrth Vallis region, Mars: Geology, v. 35, p. 951–954, 10.1130/G23854A.1.

Michalski JR, Poulet F, Loizeau D, Mangold N, Noe Dobrea EZ, Bishop JL, Wray JJ, McKeown NK, Parente M, Hauber E, Altieri F, Carrozzo FG, and Niles PB, 2010, The Mawrth Vallis region of Mars: A potential landing site for the Mars Science Laboratory (MSL) mission: Astrobiology, v. 10, p. 687–703, 10.1089/ast.2010.0491. [PubMed: 20950170]

Michalski JR, Cuadros J, Bishop JL, Darby Dyar M, Dekov V, and Fiore S, 2015, Constraints on the crystal-chemistry of Fe/Mg-rich smectitic clays on Mars and links to global alteration trends: Earth and Planetary Science Letters, v. 427, p. 215–225, 10.1016/j.epsl.2015.06.020.

Milliken RE, Ewing RC, Fischer WW, and Hurowitz J, 2014, Wind-blown sandstones cemented by sulfate and clay minerals in Gale Crater, Mars: Geophysical Research Letters, v. 41, p. 1149–1154, 10.1002/2013GL059097.

Murchie SL, Mustard JF, Ehlmann BL, Milliken RE, Bishop JL, McKeown NK, Noe Dobrea EZ, Seelos FP, Buczkowski DL, Wiseman SM, Arvidson RE, Wray JJ, Swayze GA, Clark RN, Des Marais DJ, McEwen AS, and Bibring J-P, 2009, A synthesis of Martian aqueous mineralogy after 1 Mars year of observations from the Mars Reconnaissance Orbiter: Journal of Geophysical Research. Planets, v. 114, 10.1029/2009JE003342.

Mustard JF, Murchie SL, Pelkey SM, et al., 2008, Hydrated silicate minerals on Mars observed by the Mars Reconnaissance Orbiter CRISM instrument: Nature, v. 454, p. 305–309, 10.1038/nature07097. [PubMed: 18633411]

Noe Dobrea EZ, Bishop JL, McKeown NK, Fu R, Rossi CM, Michalski JR, Heinlein C, Hanus V, Poulet F, Mustard RJF, Murchie S, McEwen AS, Swayze G, Bibring J-P, Malaret E, and Hash C, 2010, Mineralogy and stratigraphy of phyllosilicate-bearing and dark mantling units in the greater Mawrth Vallis/west Arabia Terra area: Constraints on geological origin: Journal of Geophysical Research. Planets, v. 155, E00D19, 10.1029/2009JE003351.

Noe Dobrea E, Michalski J, and Swayze G, 2011, Aqueous mineralogy and stratigraphy at and around the proposed Mawrth Vallis landing site: New insights into the aqueous history of the region: Mars, v. 6, p. 324–6.

Poulet F, Bibring J-P, Mustard JF, Gendrin A, Mangold N, Langevin Y, Arvidson RE, Gondet B, and Gomez C, and the Omega Team, 2005, Phyllosilicates on Mars and implications for early martian climate: Nature, v. 438, p. 623–627, 10.1038/nature04274. [PubMed: 16319882]

Poulet F, Arvidson RE, Gomez C, Morris RV, Bibring J-P, Langevin Y, Gondet B, and Griffes J, 2008, Mineralogy of Terra Meridiani and western Arabia Terra from OMEGA/MEx and implications for their formation: Icarus, v. 195, p. 106–130, 10.1016/j.icarus.2007.11.031.

Poulet F, Carter J, Bishop JL, Loizeau D, and Murchie SM, 2014, Mineral abundances at the final four curiosity study sites and implications for their formation: Icarus, v. 231, p. 65–76, 10.1016/j.icarus.2013.11.023.

Pye K, 1995, The nature, origin and accumulation of loess: Quaternary Science Reviews, v. 14, p. 653–667, 10.1016/0277-3791(95)00047-X.

Seelos FP, 2011, CRISM data processing and analysis products update: Calibration, correction, and visualization: 42nd Lunar Planetary Science Conference, March 7–11, The Woodlands, Texas, USA, Lunar and Planetary Institute, abstract no. 1438.

Stack KM, Edwards CS, Grotzinger JP, Gupta S, Sumner DY, Calef III FJ, Edgar LA, Edgett KS, Fraeman AA, Jacob SR, Le Deit L, Lewis KW, Rice MS, Rubin D, Williams RME, and Williford KH, 2016, Comparing orbiter and rover image-based mapping of an ancient sedimentary environment, Aeolis Palus, Gale crater, Mars: Icarus, v. 280, p. 3–21, 10.1016/j-icarus.2016.02.024.

Sun VZ, and Milliken RE, 2015, Ancient and recent clay formation on Mars as revealed from a global survey of hydrous minerals in crater central peaks: Journal of Geophysical Research. Planets, v. 120, p. 2293–2332, 10.1002/2015JE004918.

Viviano CE, and Moersch JE, 2013, Using THEMIS data to resolve the discrepancy between CRISM/OMEGA and TES modeled phyllosilicate abundance in Mawrth Vallis: Icarus, v. 226, p. 497–509, 10.1016/j.icarus.2013.06.005.

Viviano-Beck CE, Seelos FP, Murchie SL, Kahn EG, Seelos KD, Taylor HW, Taylor K, Ehlmann BL, Wisemann SM, Mustard JF, and Morgan MF, 2014, Revised CRISM spectral parameters and summary products based on the currently detected mineral diversity on Mars: Journal of Geophysical Research. Planets, v. 119, 10.1002/2014JE004627.

Wilhelm MB, Bishop JL, Wray JJ, and Ojha L, 2013, Structural variation in the ancient phyllosilicates at Mawrth Vallis: 44th Lunar Planetary Science Conference, March 18–22, The Woodlands, Texas, USA, Lunar and Planetary Institute, abstract no. 2440.

Williams RME, Malin MC, Stack KM, and Rubin DM, 2018, Assessment of Aeolis Palus stratigraphic relationships based on bench-forming strata in the Kylie and the Kimberley regions of Gale crater, Mars: Icarus, v. 309, p. 84–104, 10.1016/j.icarus.2018.02.028.

Wray JJ, Ehlmann BL, Squyres SW, Mustard JF, and Kirk RL, 2008, Compositional stratigraphy of clay-bearing layered deposits at Mawrth Vallis, Mars: Geophysical Research Letters, v. 35, 10.1029/2008GL034385.

Wray JJ, Murchie SL, Squyres SW, Seelos FP, and Tornabene LL, 2009, Diverse aqueous environments on ancient Mars revealed in the southern highlands: Geology, v. 37, p. 1043–1046, 10.1130/G30331A.1.

Wray JJ, Squyres SW, Roach LH, Bishop JL, Mustard JF, Noe Dobrea EZ, 2010, Identification of the Ca-sulfate bassanite in Mawrth Vallis, Mars: Icarus, v. 209, p. 416–21, 10.1016/j.icarus.2010.06.001.

Zolotov MY, and Mironenko MV, 2016, Chemical models for martian weathering profiles: Insights into formation of layered phyllosilicate and sulfate deposits: Icarus, v. 275, p. 203–220, 10.1016/j.icarus.2016.04.011.

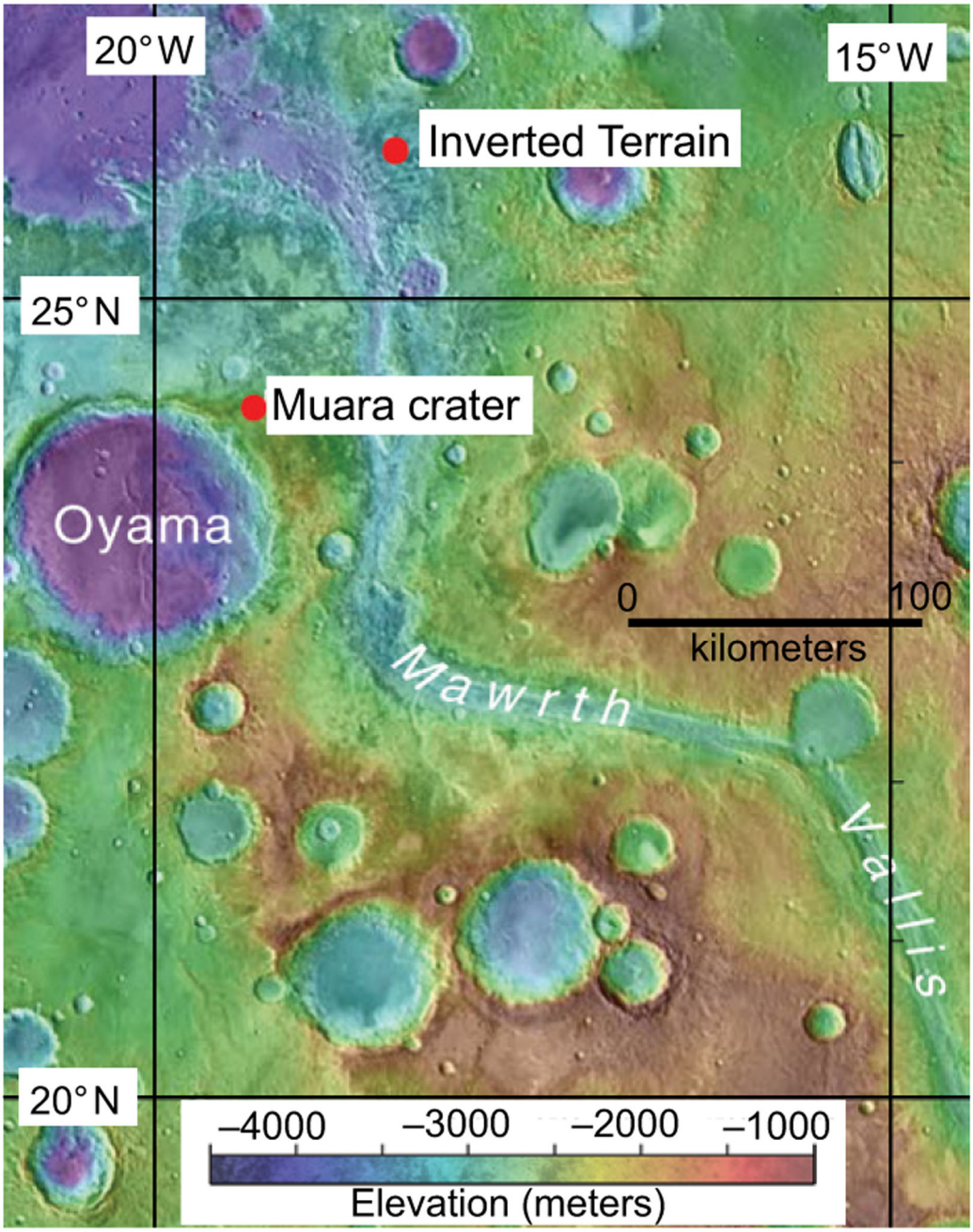

Figure 1.
Shaded relief map of the Mawrth Vallis region, Mars, showing the location of the study areas at Muara crater and the inverted terrain. MOLA (Mars Orbiter Laser Altimeter) Science Team, NASA.

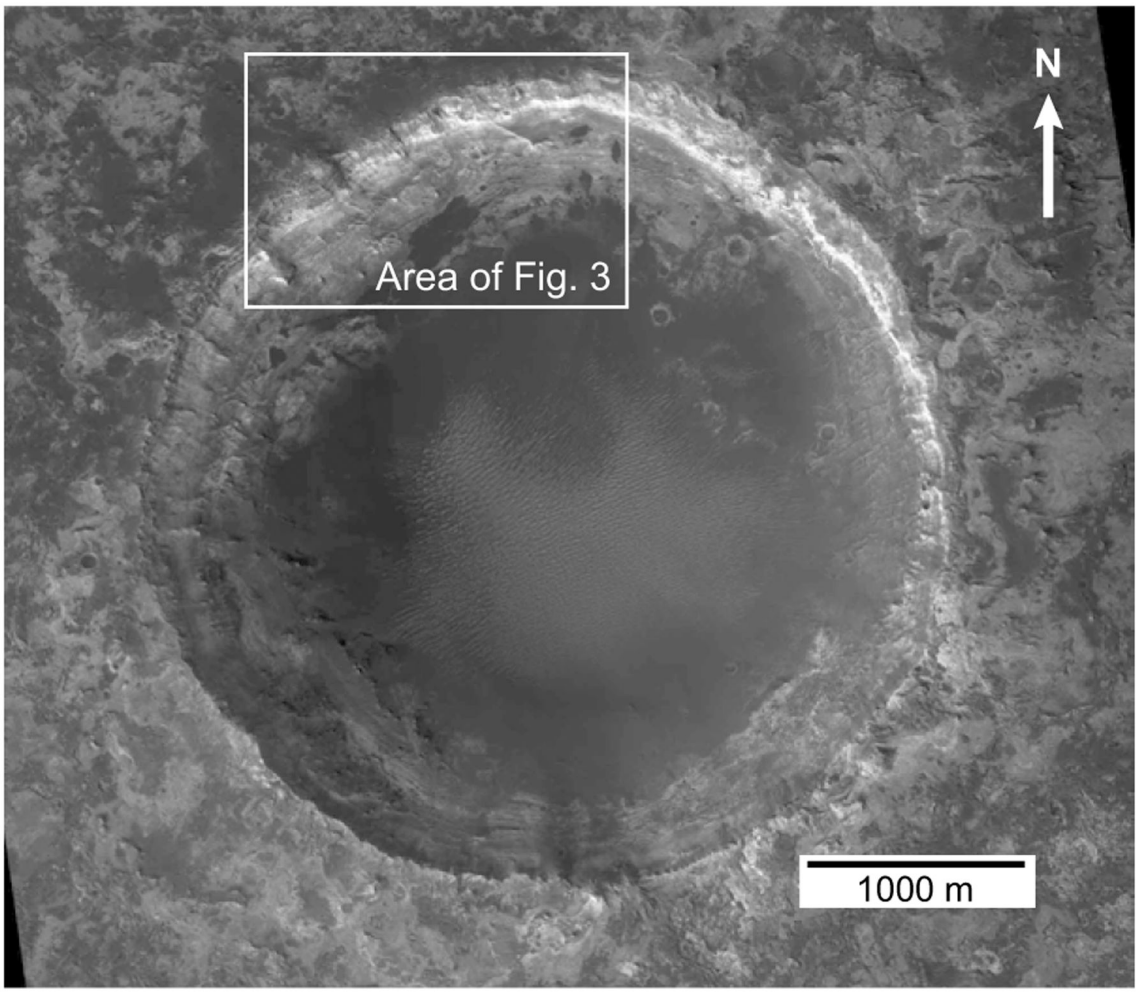

Figure 2.
Muara crater, Mars, showing the field of windblown dunes covering the crater floor (medium to dark) and bedrock outcrops of the Mawrth Vallis Group (medium to very light) around the crater walls. NASA HiRISE image PSP_004052_2045.

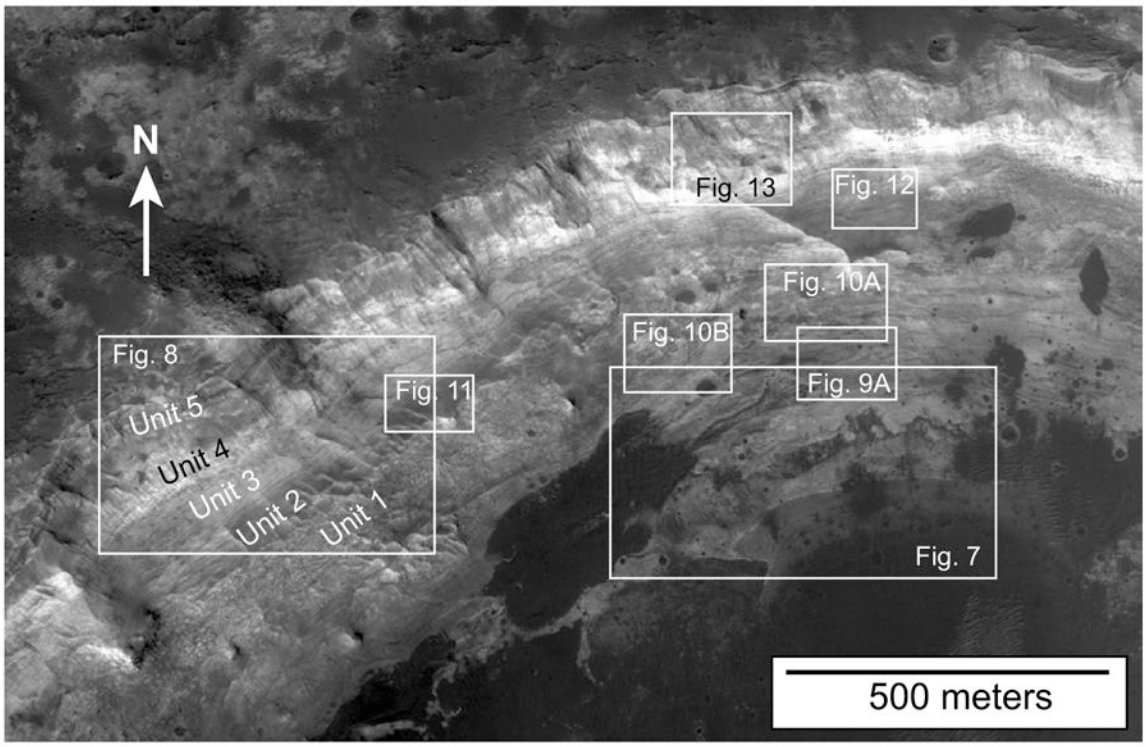

Figure 3.

Northwest wall of Muara crater, Mars, enlarged from HiRISE image PSP_004052_2045, showing outcrops of the Mawrth Vallis Group subdivided into units 1 through 5, a thin regional caprock of what is probably basalt, and the locations of other figures. The prominent light-toned band is the aluminosilicate-, clay-rich Unit 4. The dark-toned areas to the lower right and lower center are covered by windblown sand.

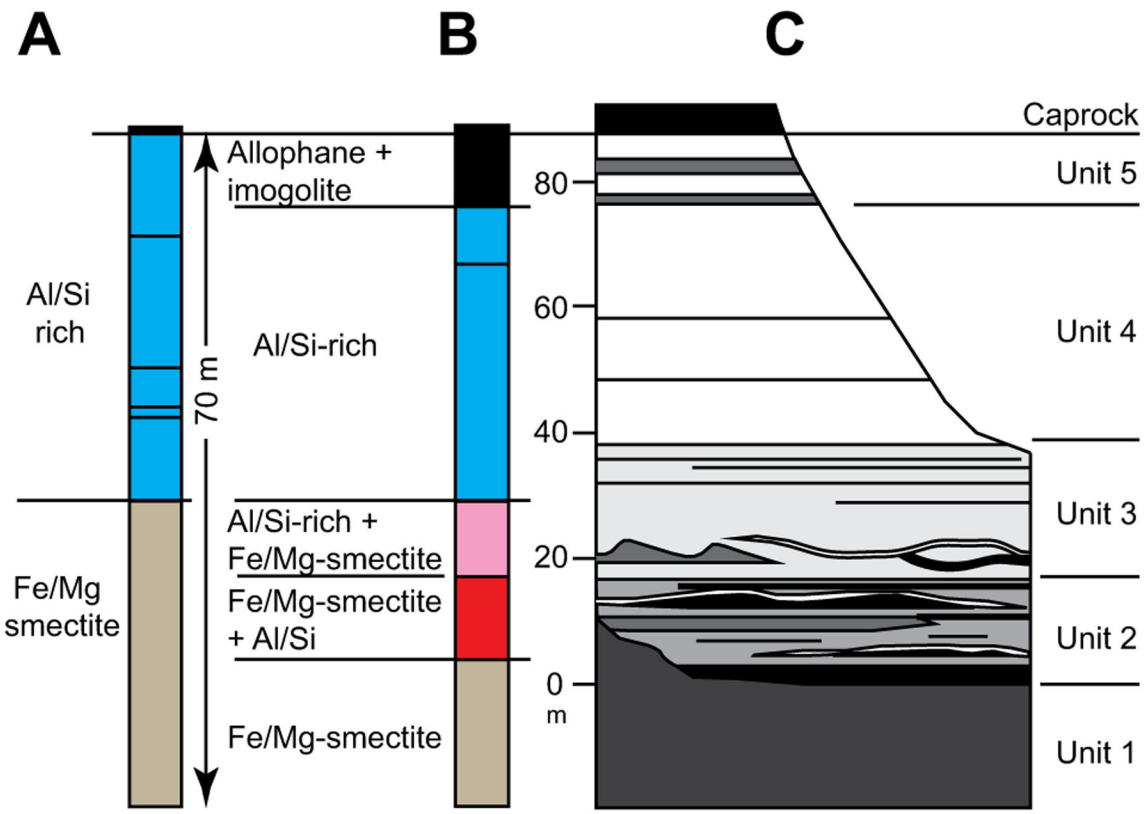

Figure 4.

Stratigraphy of the Mawrth Vallis Group, Mars. (A) Stratigraphic divisions of (A) Loizeau et al. (2010) and (B) Bishop et al. (2013b). (C) Stratigraphic subdivisions recognized in the present study in Muara crater. Correlations between the spectral divisions of (A) and (B) and the lithologic divisions of the present study are approximate.

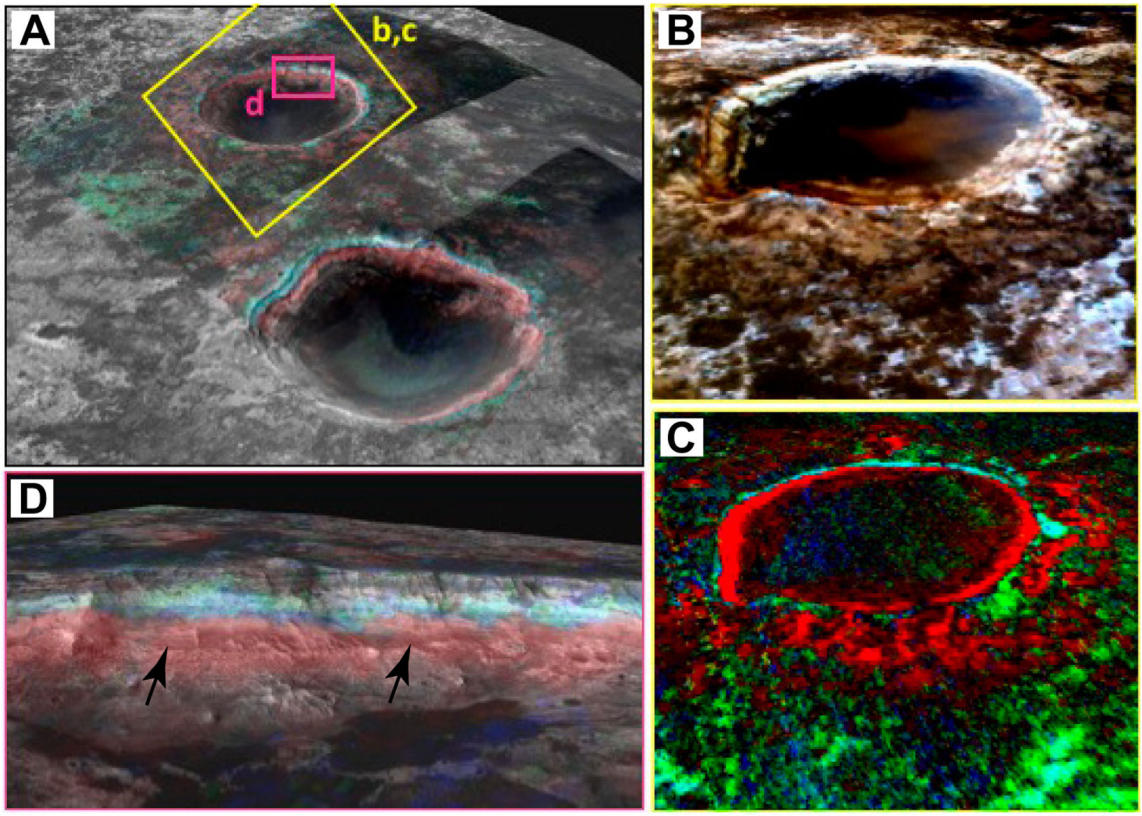

Figure 5.

Phyllosilicate zones in and around Muara crater, Mars, 3.8 km in diameter. (A) 3-D view from CRISM image FRT000094F6 highlighting the phyllosilicates in Muara (far) and Tarrafal (close) craters. CRISM image with 5× vertical exaggeration is draped over a high resolution stereo camera image (HRSC). (credit: C. Gross, Freie Universitat-Berlin, Germany). The colors are from CRISM parameters (Red = bd2290, Green = bd2190, Blue = bd2210_2) as defined by Viviano-Beck et al. (2014). The reddish areas are spectrally dominated by Fe/Mg smectite, the bluish areas by Al-phyllosilicates, and the greenish areas by poorly crystalline aluminosilicates similar to allophane. (B) 3-D view of Muara crater showing distribution of phyllosilicate-rich units (Red = R600, Green = R530, Blue = R440). CRISM FRT000096F6 image with 5× vertical exaggeration is draped over MOLA topographic image. (C) 3-D CRISM view of phyllosilicate-rich units with colors as in A. CRISM image with 5× vertical exaggeration is draped over MOLA topographic image. (D) Oblique image showing a horizontal view of the NW wall of Muara crater with colors as in A (after Bishop et al., 2018). The phyllosilicate zones from CRISM are superimposed on HiRISE image PSP_004052_2045 in grayscale overlain on a HiRISE digital terrain model. The jagged edge of the red/blue contact reflects the pixelation due to the lower resolution of the CRISM image. Note that the lower part of the Fe/Mg smectite zone lies 50–60 m below the contact of units 1 and 2 (arrows). Lower parts of Unit 1 show little alteration. The uppermost part of the crater wall above the blue Al-phyllosilicate zone corresponds to Unit 5 and is characterized by allophane and imogolite. CRISM parameters colorizing each image are as defined by Viviano-Beck et al. (2014).

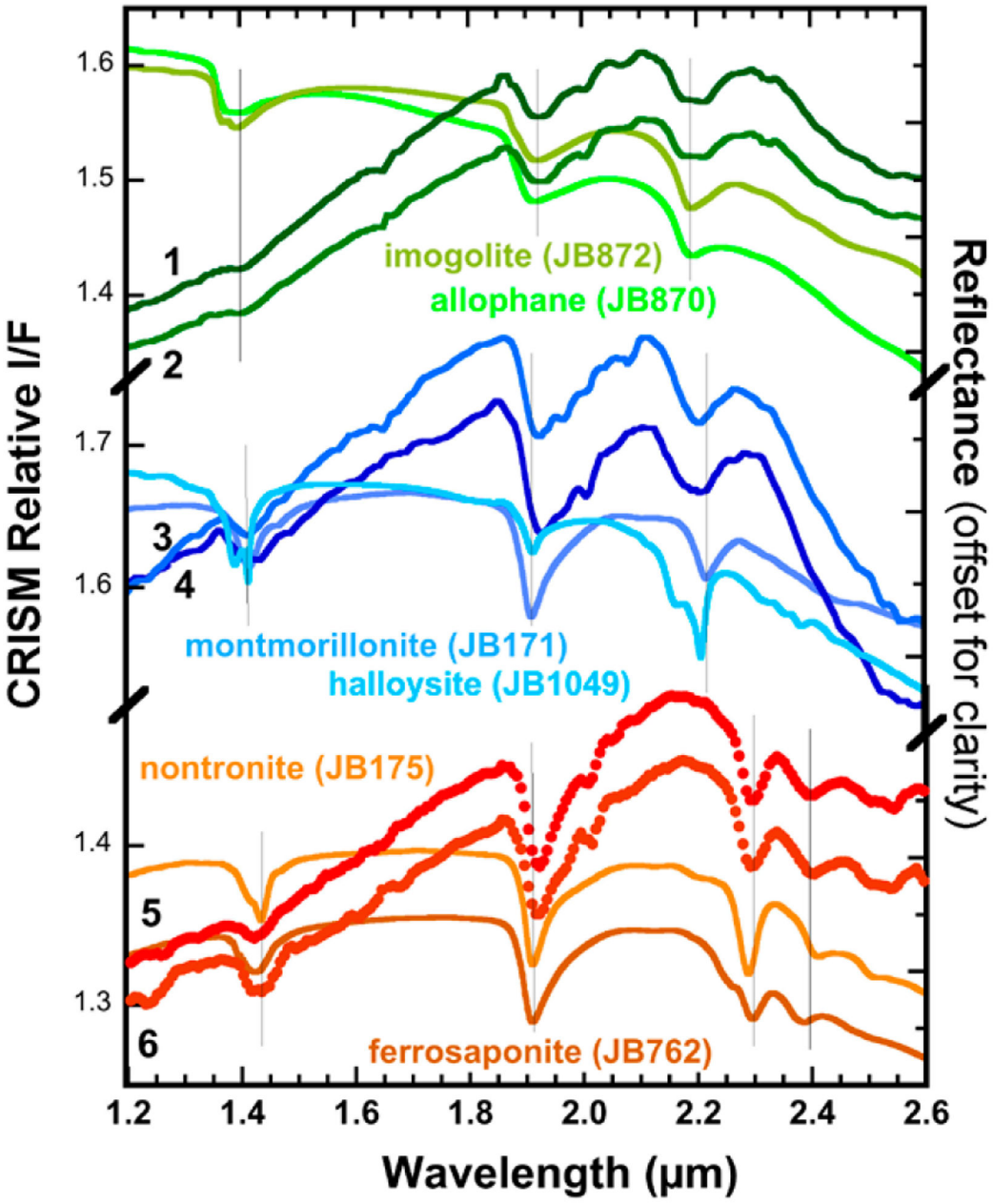

Figure 6.

I/F CRISM spectra from image FRT000094F6 representing the units colored green, blue, and red in Figure 5C. Spectra 1 and 2 are dominated by short-range ordered aluminosilicates, spectra 3 and 4 include Al-rich phyllosilicates, and spectra 5 and 6 include Fe-rich smectites. Lab spectra of minerals/materials are shown for comparison: allophane and imogolite from Bishop et al. (2013b), montmorillonite and halloysite from Bishop et al. (2008b), and nontronite and Fe/Mg smectite from Bishop et al. (2008a, 2008b). Grey vertical lines mark the spectral features due to H_2O and metal-OH in the crystal structure that are used to characterize the phyllosilicates and related materials present in the regions associated with these spectra.

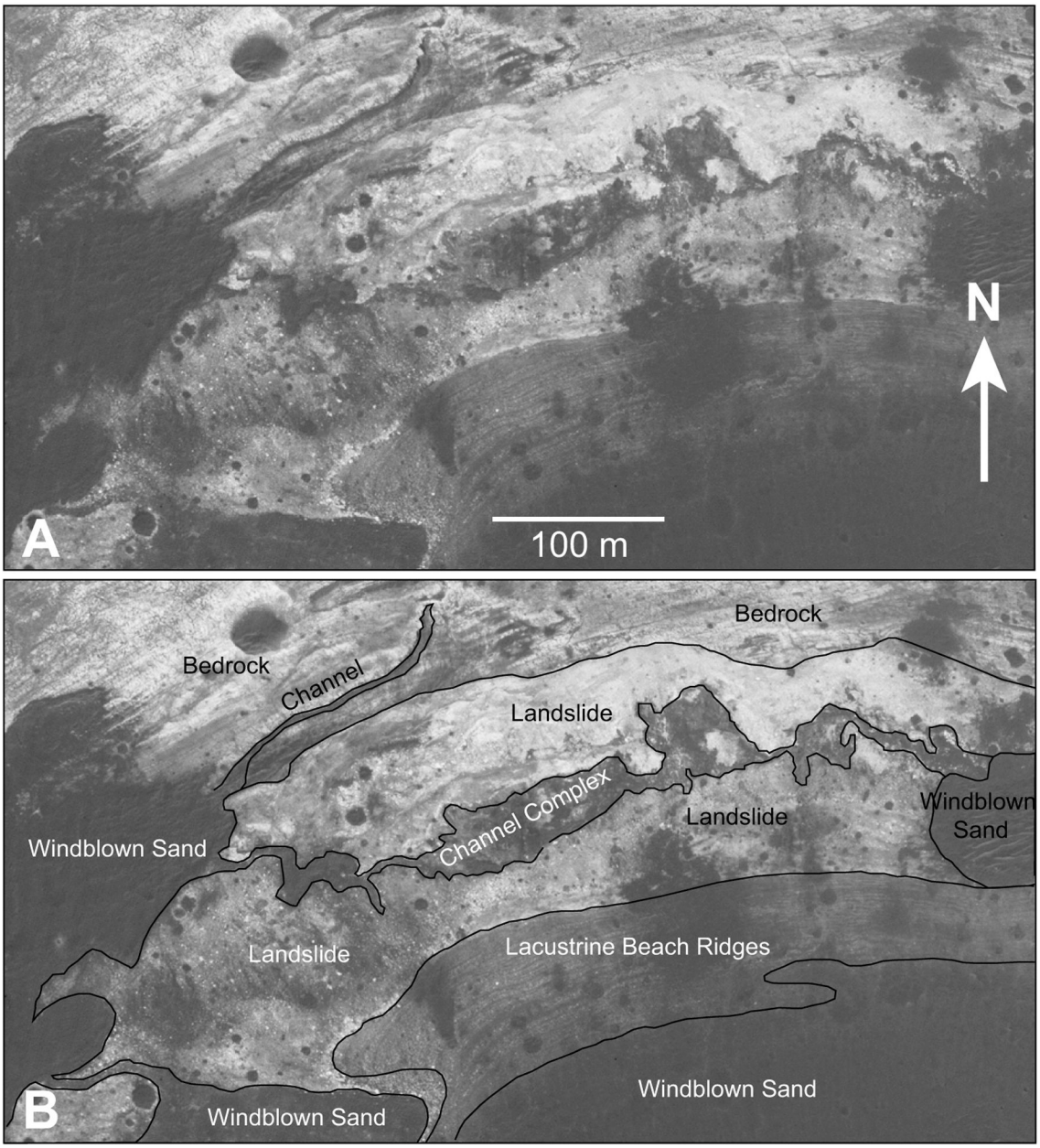

Figure 7.

Lower part of the NW crater wall and adjacent crater floor of Muara crater, Mars. (A) With features unlabeled. (B) With features labeled showing large landslides, runoff channels, beach ridges marking old shorelines around crater lake, and later windblown sand. This part of the wall is composed mainly of bedrock Unit 1 of the Mawrth Vallis Group. Lower on the slope, bedrock is overlain by landslides, some of which probably represent the edge of the breccia lens formed at the time of cratering. Water runoff subsequently cut local channels across the Unit 1 outcrops and the landslide breccia. This runoff resulted in the formation of a transient crater lake that gradually dried, leaving a set of very coarse-grained beach ridges as the shoreline retreated.

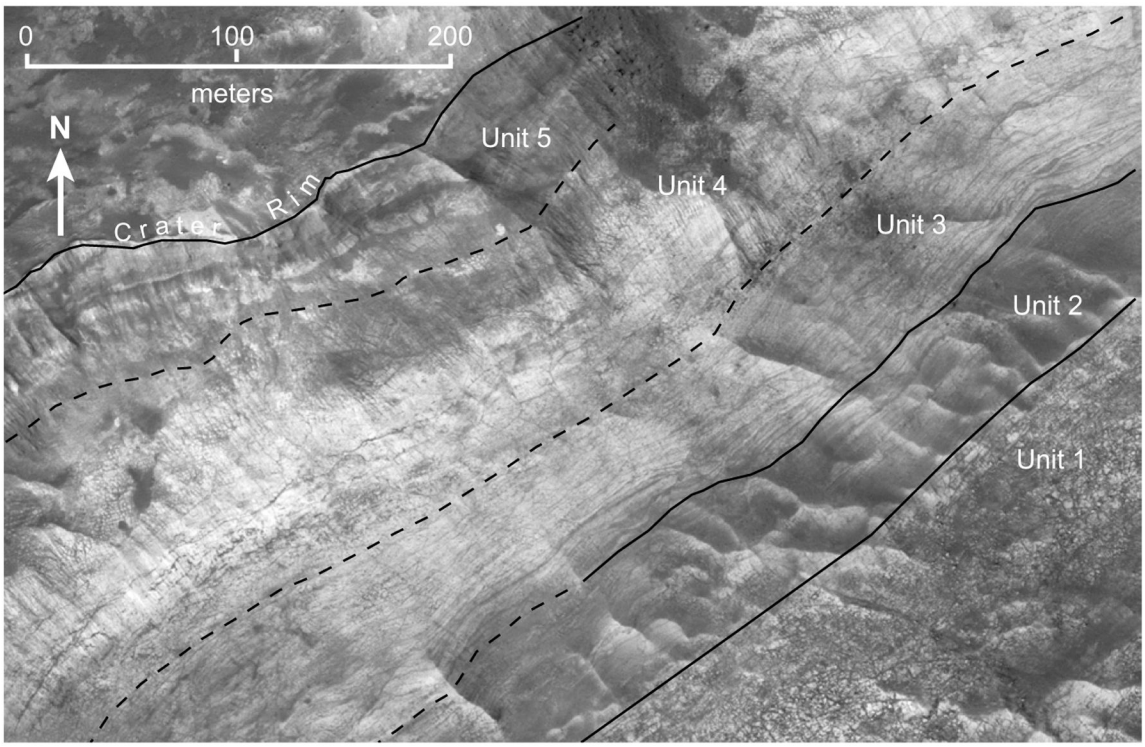

Figure 8.
Northwest wall of Muara crater, Mars, showing main subdivisions of the Mawrth Vallis Group.

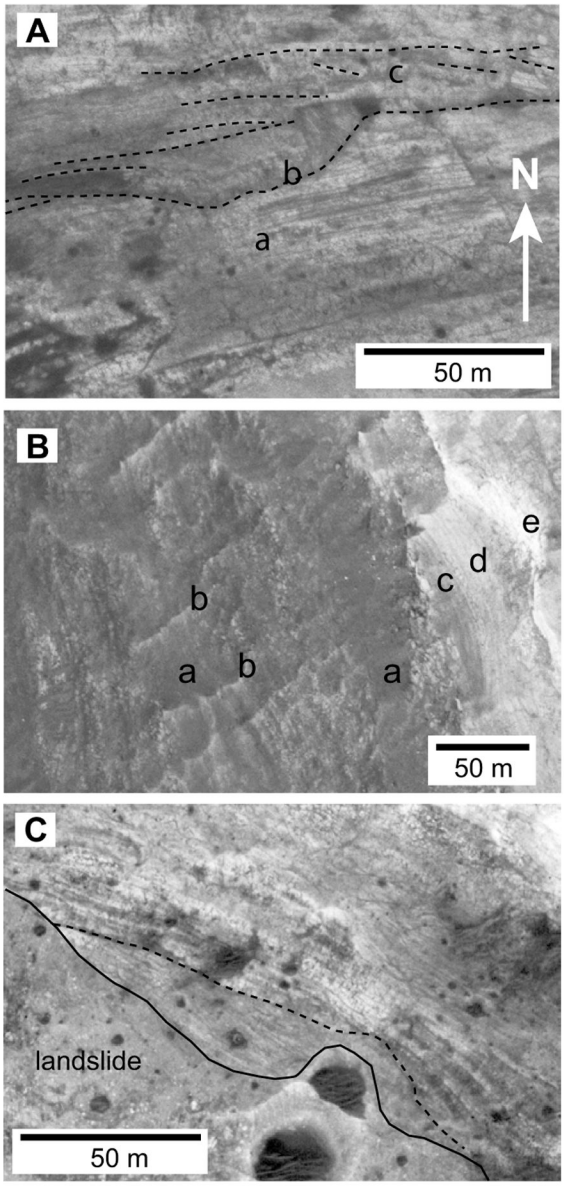

Figure 9.

Unit 1 of the Mawrth Vallis Group (MVG) in Muara crater, Mars. (A) Lower part of Unit 1 of the MVG on the northwest crater wall showing the fine layering parts of this section (a), a possible erosional channel (b), and cross-sets that may be aeolian beds (c). (B) A portion of the Mawrth Vallis Group on the eastern wall of Muara crater. The upper part of Unit 1 occupies most of the photo. It shows crude layering and the interstratification of resistant and weaker units. Many areas are covered by patches of younger windblown sand (a) and the area is crossed by irregular wind-sculpted ridges (b). There is some divergence of bedding in Unit 1 but no conspicuous erosional channels or steeply dipping layering. Overlying MVG units 2 (c), 3 (d), and 4 (e) lie along the right side of the photo. Details have been sharpened. (C) Lower part of NE crater wall showing major truncation surface (dashed line) in the lower part of Unit 1.

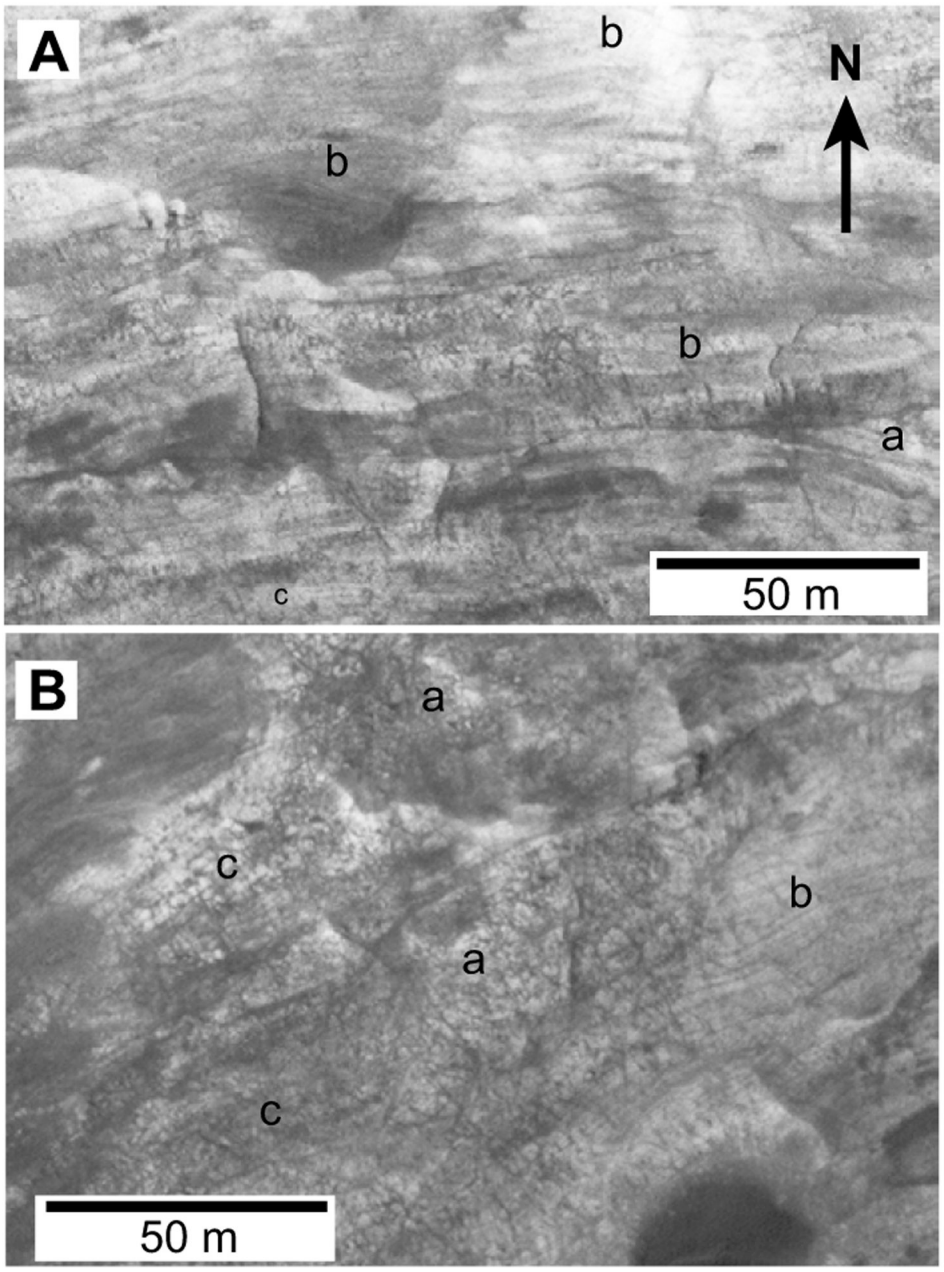

Figure 10.

Unit 1 on north wall of Muara crater, Mars. (A) Middle to upper part of Unit 1 showing thicker, crude layering that includes large cross sets (a) and undulating layering (b). This sequence may consist largely of windblown sand. The thinner layering of the lower part of Unit 1 can be seen at the bottom of the photo (c). (B) Massive fractured rock at the top of Unit 1 (a). Some areas of well-defined layering are laterally equivalent to fractured rock (b) and some layering can be seen through fractures (c). See Figure 3 for location.

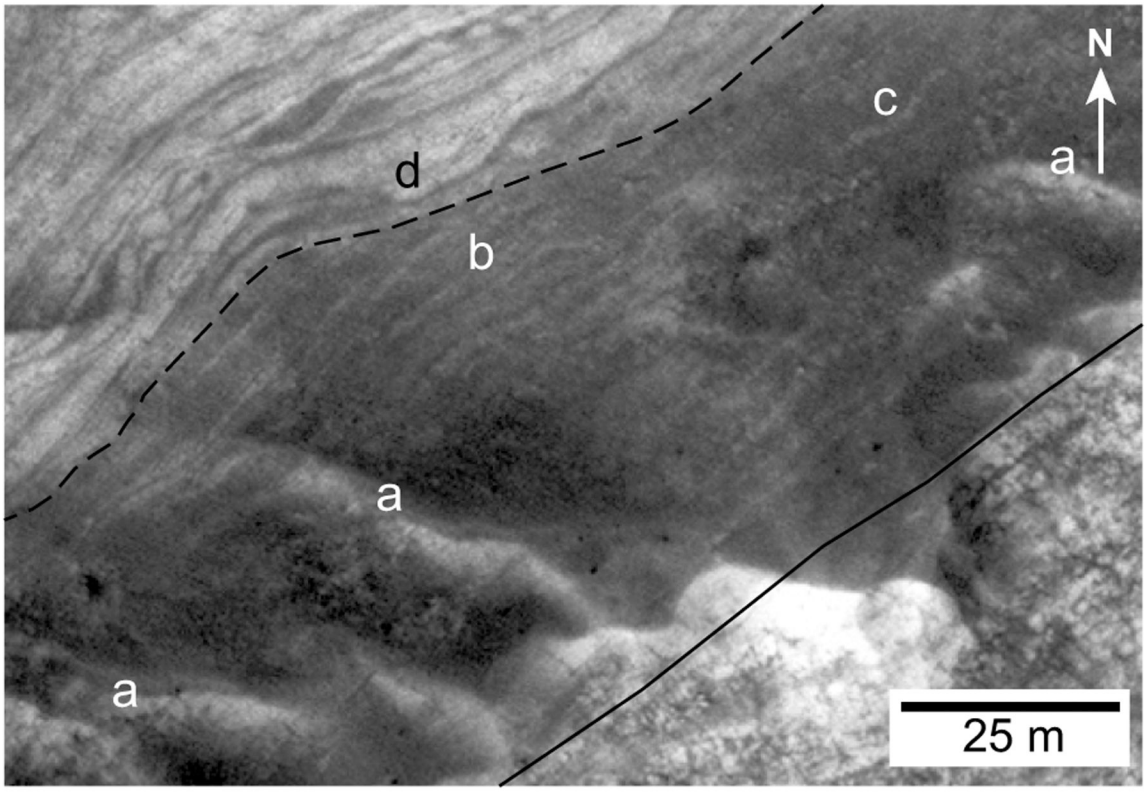

Figure 11.

Uppermost Unit 1 (light, lower right), Unit 2 (dark band, center), and lower Unit 3 (light banded, upper left) of the Mawrth Vallis Group, northwest wall of Muara crater, Mars. The crater wall slopes from upper left to lower right. Low, sharp-crested ridges (a), illuminated on their SW sides, extend up and down the slope. The blocky weathering of Unit 1 is overlain with a sharp contact by the more massive, dark layer of lowest Unit 2 (solid line). The bulk of Unit 2 shows medium- to light-toned layers, <1 to ~2 m thick, interbedded with slightly darker layers and very dark thin layers. Most layers are relatively flat, with apparent undulations reflecting topographic irregularities, but some show low peaks (immediately right of b) and swales (c). The complex stratigraphy of the lower part of Unit 3 is evident, with an unconformity between units 2 and 3 (dashed line) and internal erosional unconformities (d), discontinuous strata, pinch and swell features, and draping units. Contrast and sharpness enhanced.

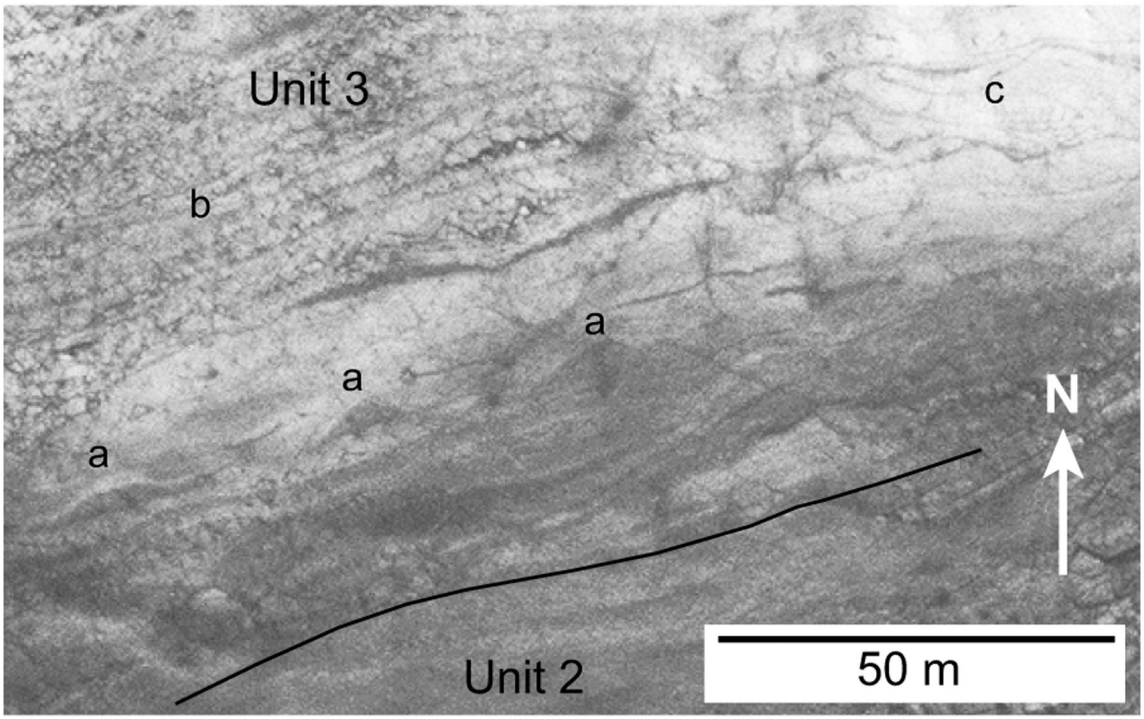

Figure 12.

Part of the northern wall of Muara crater showing the upper part of Unit 2 and most of Unit 3 of the Mawrth Vallis Group, Mars. The lower part of Unit 3 shows a train of well-developed, lenticular, dune-like features (a) composed of dark sandy(?) sediment that are draped by light-toned material. Above the zones of dunes and lenticular dark layers, Unit 3 consists of tabular light-toned layers separated by very thin, continuous layers of dark material (b), many of which appear thicker than they actually are because of younger, dark, windblown sand accumulating on small benches marking bedding surfaces. A set of closely spaced joints produces saw-tooth like fractures of the light-toned layers that are filled by dark windblown(?) sediment. The tabular light layers traced to the right show swales and features suggesting possible dunes (c). For location of this area, see Figure 3.

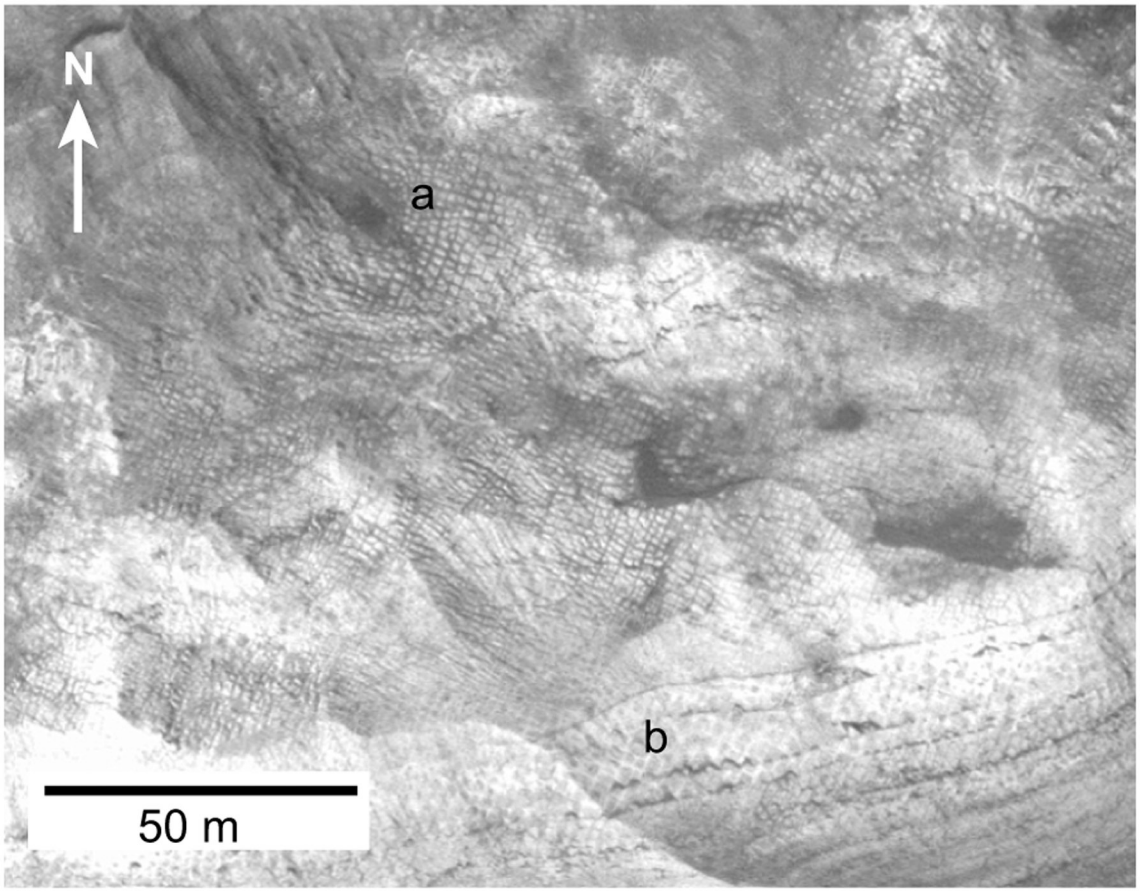

Figure 13.

Joint set (a) in the upper wall of Muara crater, Mars. This view is immediately higher on the crater slope than the view in Figure 12 and includes Unit 4 (light toned) and overlying Unit 5, which is largely covered by dark debris. The joints and bedding form saw-tooth fractures and displaced blocks (b).

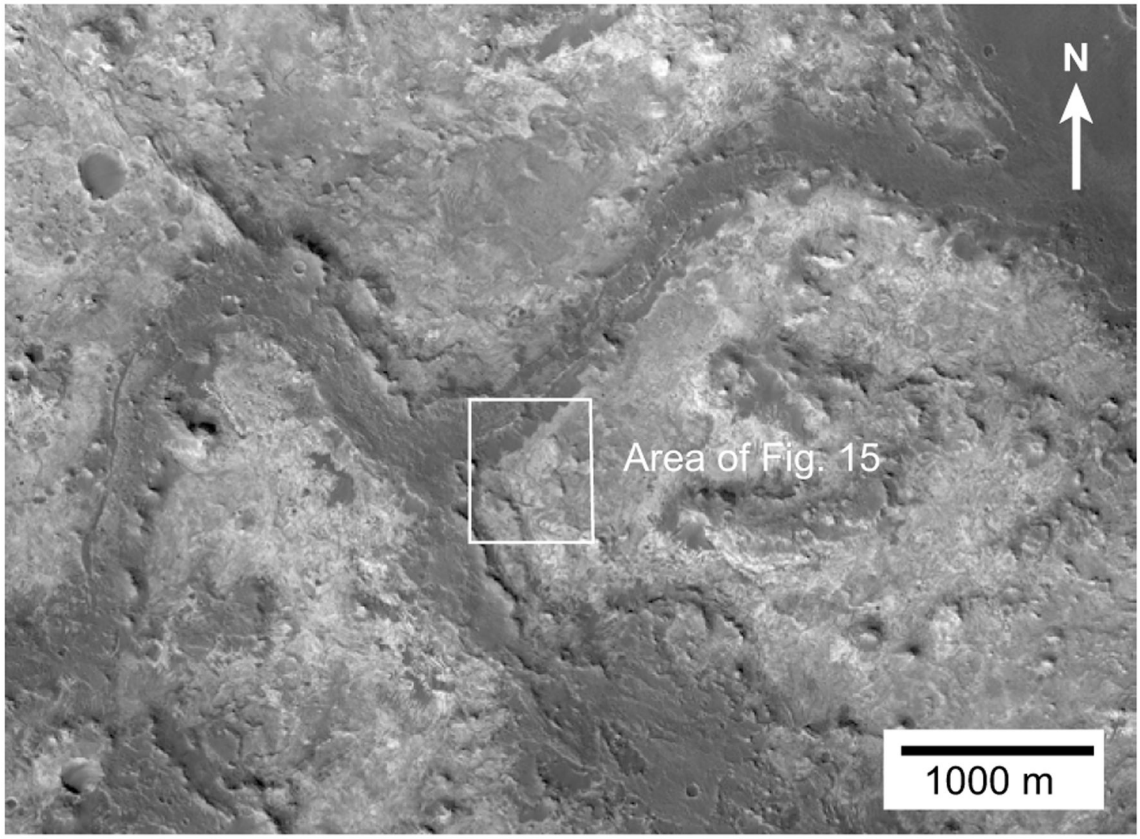

Figure 14.
Location photo for the inverted terrain study area, Mars. The area is characterized by topographically high, sinuous plateaus capped by dark rock, probably basalt, and low, light- to medium-toned valleys underlain by phyllosilicate-bearing rocks of the Mawrth Vallis Group.

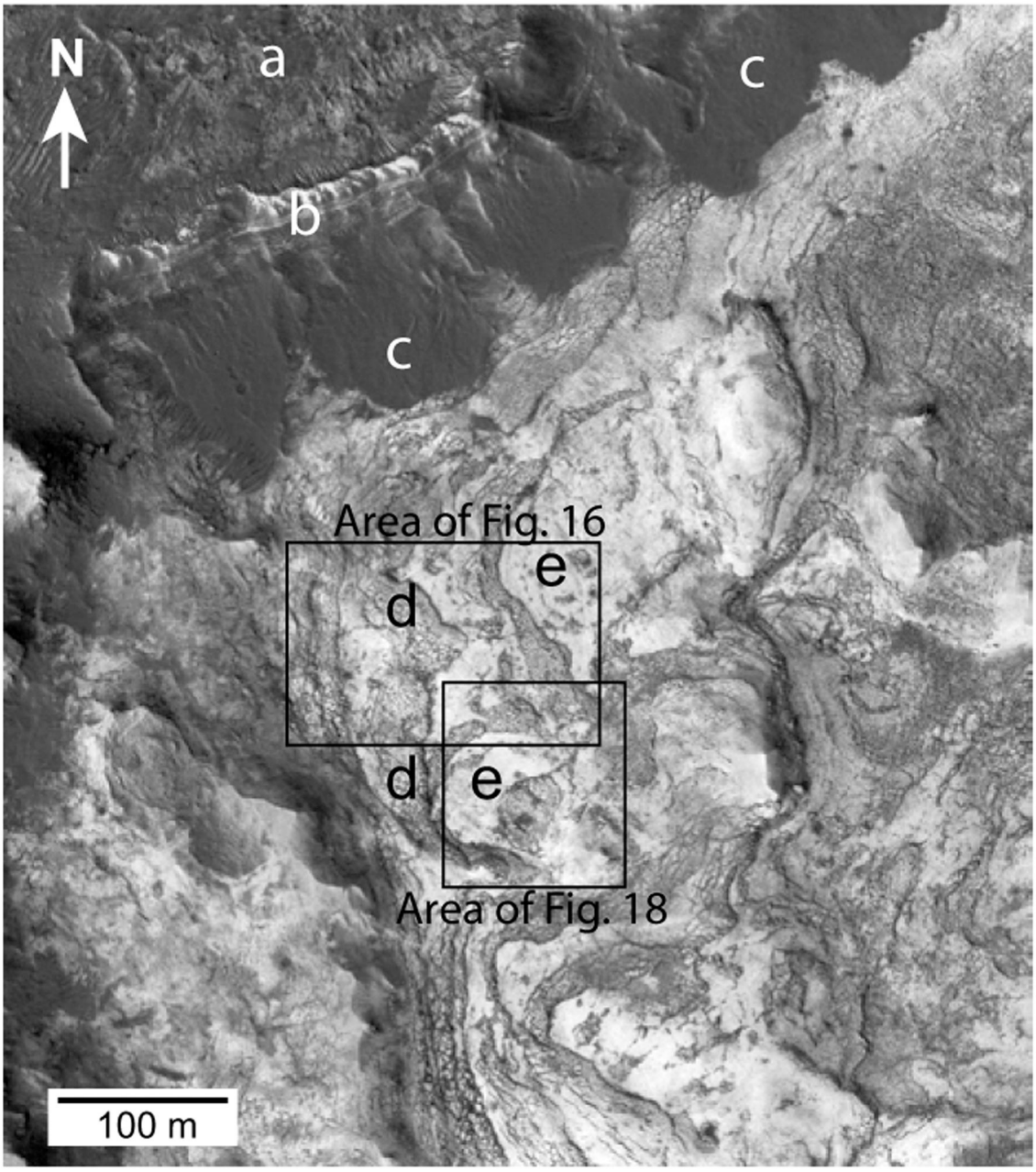

Figure 15.

Study area in the inverted terrain, Mars. A large, low, essentially uncratered area of light-toned rock of Unit 4 of the Mawrth Vallis Group is bounded to the north and west by a plateau capped by dark-toned rock, probably basalt (a). The plateau is flanked by cliffs of exposed Unit 5 of the Mawrth Vallis Group (b) and, lower on the slope, by accumulations of dark sandy or gravelly debris (c). Unit 4 outcrops on the valley floor (light toned) show zones of heavily broken rock (d) separated by smooth areas of unbroken light-toned rock (e).

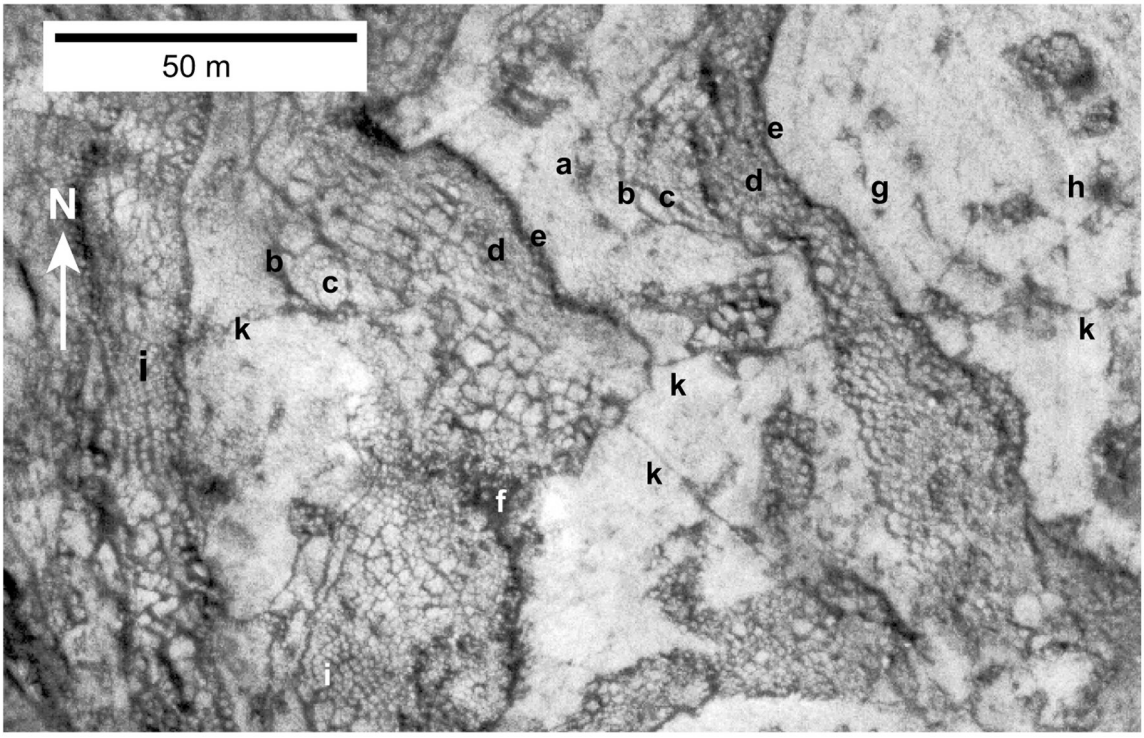

Figure 16.

Area in the inverted terrain showing zones of rubble and brecciated rock separated by zones of smooth, intact rock. The rubble zones have developed by failure, sliding, and brecciation of surface layers composed mainly of light-toned sediments. Some of these failures display a distinct downslope zonation including locally a headward fracture (a), a head scarp (b), and an upper zone of large, little displaced blocks (c) grading downslope into finer rubble zones to a front of small, jumbled blocks probably representing debris-flow material (d). The front of the slides are distinct, shadowed scarps (e). Where most of the light-toned layers have been removed there are accumulations of darker sediment (f). On the right are a series of fractures (g and h) parallel to the slide front. In some areas, brecciation involved fracturing along polygon boundaries in the strongly patterned ground (i). A few through-going fractures are present (k). Enhanced contrast and sharpened. See Figure 15 for location.

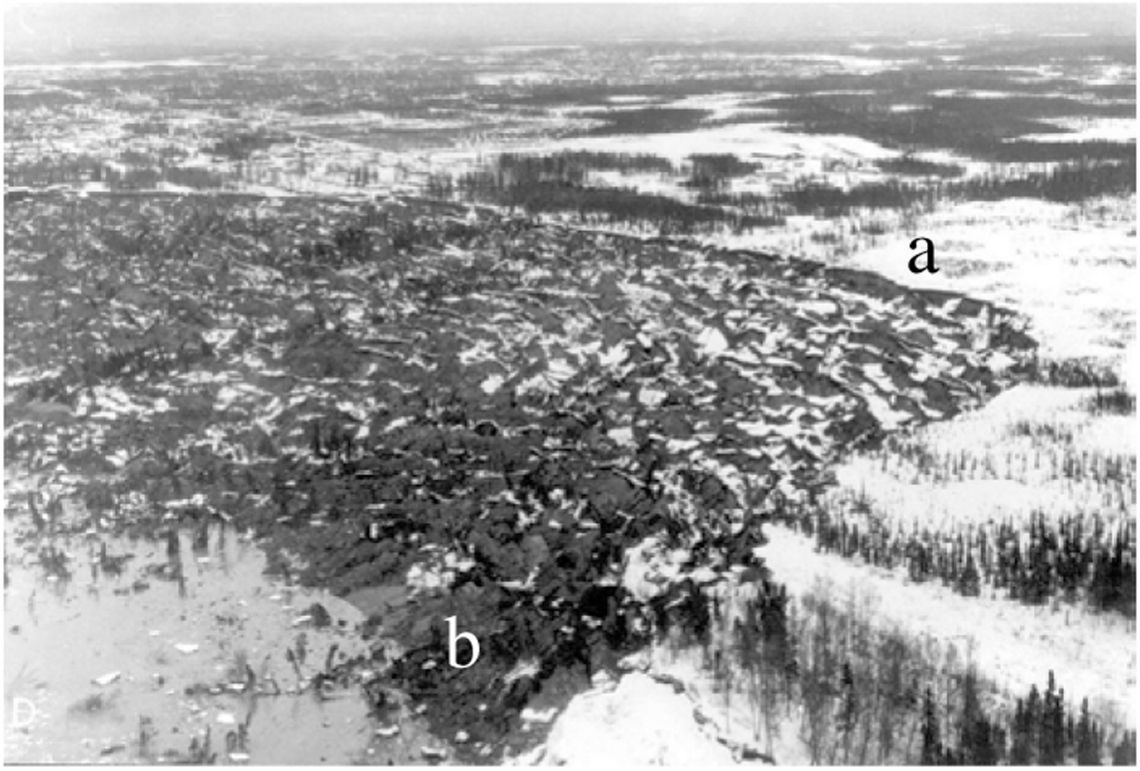

Figure 17.

Landslide triggered by the 27 March 1964, earthquake in Anchorage, Alaska, USA. Note head scarp (a), down-dropped blocks in upper part of slide, and debris-flow-like toe of slide (b). Photo by A. Grantz, U.S. Geological Survey Circular 491.

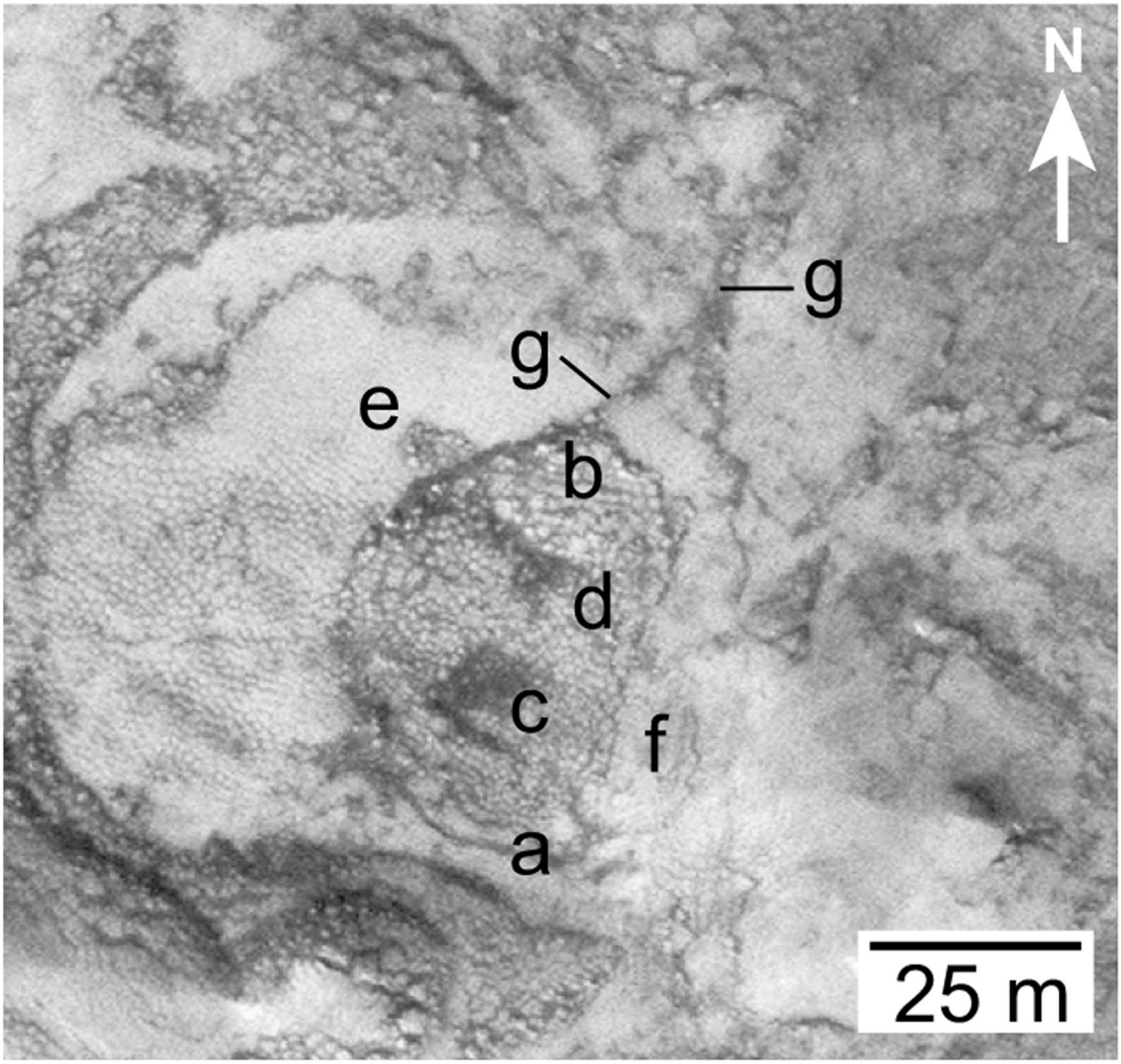

Figure 18.

Small slide area of brecciated Unit 4 surrounded by largely intact, strongly patterned ground. The slide shows a headward scarp (a), a downslope end composed of larger blocks (b), and a middle area that includes two topographic low areas covered with dark, finer, probably sandy sediment (c and d). (d) is at the head of a low area with abundant dark sediment that extends as a low-channel-like feature to the NW. It is characterized by dark sediment and isolated blocks of Unit 4. One small debris-flow lobe extends 8–10 m out onto the adjacent flat area of patterned ground (e). The fine fractures characterizing the mid-part of the failure have formed along the sides of polygons in the original patterned ground. Older lobes of failed and brecciated rock (f) appear to be covered by a thin layer of fine light-toned, possibly windblown dust and silt. There are irregular ribbons of darker material and isolated larger blocks (g) extending downslope from the tips of the failures that appear to mark a runoff channel. See Figure 15 for location.

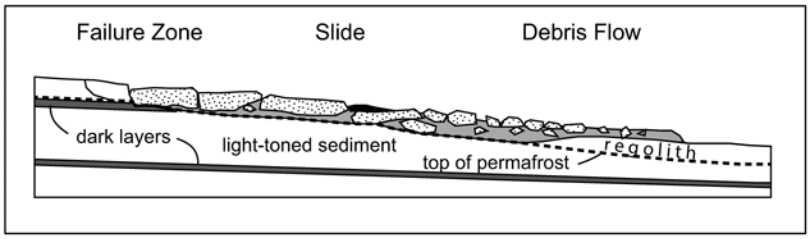

Figure 19.

Inferred origin of the breccia zones in the inverted terrain study area, Mars. Outcropping rock includes thicker light-toned layers of Unit 4 composed of fine silty and clayey sediments and possibly thinner, probably granular, dark layers. Both are saturated with water ice. There is a permafrost substrate (surface indicated by dashed line) overlain by the lowest light-toned sediment and a capping layer of debris and regolith. Partial melting at the top of the permafrost results in destabilization of the overlying bedrock and surface debris, failure, and sliding. Progressive upslope stepping of the headward fractures exposes additional rocks to sublimation and possible melting, promoting additional downslope sliding. Downslope the size and proportion of light blocks diminishes due to block fracturing, melting, and sublimation. Displaced blocks are shown stippled; the finer matrix in gray.